First-principles and Monte Carlo study of magnetostructural transition and magnetocaloric properties of $Ni_{2+x}Mn_{1-x}Ga$

V. D. Buchelnikov,[1] V. V. Sokolovskiy,[1,2] H. C. Herper,[2] H. Ebert,[3] M. E. Gruner,[2] S. V. Taskaev,[1] V. V. Khovaylo,[4] A. Hucht,[2] A. Dannenberg,[2] M. Ogura,[5] H. Akai,[5] M. Acet,[2] and P. Entel[2]

[1]*Condensed Matter Physics Department, Chelyabinsk State University, 454001 Chelyabinsk, Russia*

[2]*Faculty of Physics and Center for Nanointegration, CeNIDE, University of Duisburg–Essen, D-47048 Duisburg, Germany*

[3]*Department of Chemistry and Biochemistry/Physical Chemistry, LMU Munich, Butenandtstraße 11, D-81377 Munich, Germany*

[4]*National University of Science and Technology "MISiS," Moscow 119049, Russia*

[5]*Department of Physics, Osaka University, 1-1 Machikaneyama, Toyonaka, Osaka 560-0043, Japan*

(Received 5 December 2009; published 11 March 2010)

First-principles calculations of magnetic exchange parameters of the austenitic and martensitic phases of Ni-Mn-Ga allow one to characterize this Heusler system across the phase diagram in agreement with experimental trends. The *ab initio* investigations have been combined with Monte Carlo simulations for a detailed description of the magnetic, martensitic, and magnetocaloric properties of $Ni_{2+x}Mn_{1-x}Ga$ $(0.18 \leq x \leq 0.27)$ Heusler alloys, which undergo a first-order magnetostructural phase transition. For these alloys, the calculated temperature dependence of the magnetic and lattice contributions to the total specific heat as well as the evaluation of the isothermal magnetic entropy $\Delta S_{mag}(T,H_{ext})$ and adiabatic temperature $\Delta T(T,H_{ext})$ changes around the magnetostructural transition in an external magnetic field agree fairly well with the experimental data. In particular, results for $\Delta S_{mag}(T,H_{ext})$ and $\Delta T(T,H_{ext})$ may be used to speculate about designing new magnetic Heusler alloys with better magnetocaloric properties, i.e., larger $\Delta T(T,H_{ext})$ values.

DOI: 10.1103/PhysRevB.81.094411 PACS number(s): 75.50.−y, 75.10.−b, 75.30.Sg

I. INTRODUCTION

The magnetocaloric effect (MCE) describing the reduction in the magnetic part of the total entropy upon adiabatic magnetization is an intrinsic property of any magnetic material. Nowadays, this phenomenon has attracted considerable attention due to the possibility of utilizing the MCE in room-temperature magnetic refrigeration.[1] In particular, the discovery of giant MCE in $Gd_5(Si_{1-x}Ge_x)_4$ (Ref. 2) and $MnFeP_{0.45}As_{0.55}$ (Ref. 3) has renewed the interest in materials undergoing first-order magnetic phase transitions where the frequently observed giant magnetic entropy change arises from the coupling of the magnetic to the elastic degrees of freedom.[4]

The MCE has been studied theoretically for several alloy systems in the framework of molecular-field approximation,[5] bond-proportion model, where antiparallel spins are assumed to have a different stiffness than parallel spins,[6,7] and Monte Carlo (MC) method.[8–13] Using the MC approach, the magnetocaloric properties of rare-earth silicides and Laves phase compounds could be modeled successfully. In particular, the calculated isothermal magnetic entropy (ΔS_{mag}) and adiabatic temperature (ΔT) changes in $Gd_5(Si_xGe_{1-x})_4$ $(x>0.5)$,[8] R_5Si_4 $(R=\mathrm{Gd,Tb})$,[9] RAl_2 $(R=\mathrm{Dy,Tb})$,[10] and $(Gd_xTb_{1-x})_5Si_4$ (Ref. 11) were found to be in good agreement with available experimental data. It is worthwhile to note that the above-mentioned alloys undergo a second-order magnetic phase transition. Therefore, only the magnetic subsystem has been taken into account when calculating their magnetocaloric properties. The case of first-order magnetic transition, for instance, in $La(Fe_xSi_{1-x})_{13}$ or MnAs, has so far been considered either phenomenologically[14,15] or by the bond-proportional model.[6,7]

Among the Mn-based intermetallic compounds and alloys,[16] Ni-Mn-Ga Heusler systems have received significant attention regarding their magnetic shape memory properties for compositions close to stoichiometry and, in particular, their magnetocaloric properties at off-stoichiometric compositions[17–31] [see Ref. 32 for a discussion of the MCE and its relation to shape-memory properties in ferromagnetic (FM) Heusler alloys]. Since, in particular, the Heusler alloys are cheaper than the rare-earth alloys and are also environmentally more friendly than MnAs-based materials, Ni-Mn-Ga (with a large magnetic entropy change[17,21,24,27]) is attractive for application in magnetic refrigeration.

Stoichiometric Ni_2MnGa, with the crystal structure shown in Fig. 1, undergoes a martensitic transformation on cooling below $T_m \approx 200$ K in the ferromagnetically ordered state with a Curie temperature $T_C \approx 376$ K.[33] Recent experimental studies on nonstoichiometric $Ni_{2+x}Mn_{1-x}Ga$ have revealed that both transition temperatures, T_m and T_C, are very sensitive to changes in the chemical composition as shown by the increase in T_m and decrease in T_C with Ni excess.[34–36] In the range of compositions $0.18 \leq x \leq 0.27$, structural and mag-

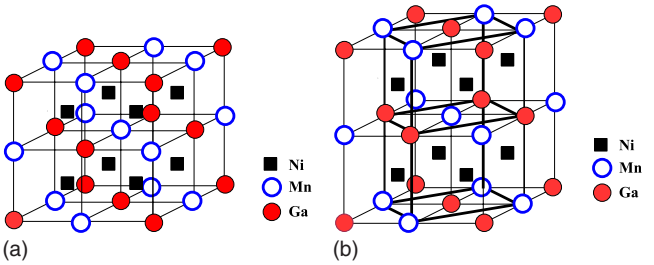

FIG. 1. (Color online) (a) The cubic $L2_1$ structure of the Heusler compound Ni_2MnGa and (b) the tetragonal $L1_0$ structure with $c/a=1.25$. Filled squares (black), open circles (blue), and filled circles (red) denote Ni, Mn, and Ga atoms, respectively. Solid lines in (b) highlight the tetragonal unit cell.

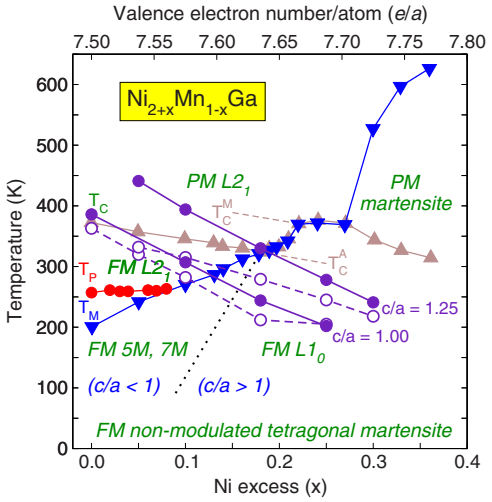

FIG. 2. (Color online) Ni-excess phase diagram showing the merging of Curie and martensitic transformation temperatures for $0.18 \leq x \leq 0.27$ (triangles up and down, respectively), which is the important region of the MCE. T_P marks the premartensitic transition. PM and FM denote the paramagnetic and ferromagnetic phases, and $L2_1$ and $L1_0$ are the cubic and tetragonal phases, respectively. The dotted line separates the modulated 5M and 7M phases with tetragonal distortion $c/a<1$ from the nonmodulated phases with $c/a>1$. Open and filled circles mark the T_C values obtained from Monte Carlo simulations and mean-field approximation using the *ab initio* J_{ij} for $c/a=1.00$ and 1.25, respectively. T_C^A and T_C^M indicate schematically the behavior of the magnetic phase transition lines if one would extrapolate (by hand) the Curie temperatures of austenite ($x<0.18$) and martensite ($x>0.27$), respectively.

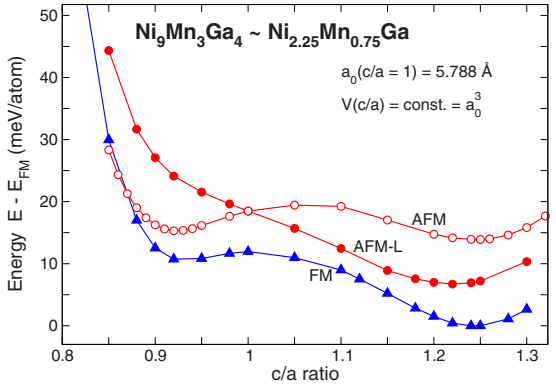

FIG. 3. (Color online) Energetics of the cubic $L2_1 \leftrightharpoons$ tetragonal $L1_0$ lattice transformation following the Bain path. The $L1_0$ structure is by 10 meV/atom lower in energy than the $L2_1$ phase. The volume has been kept constant in the c/a variation (its change is less than 0.25%). Beside the FM solution, two antiferromagnetic (AFM) solutions are shown, see text for explanation.

netic phase transitions merge together (see the phase diagram in Fig. 2). For these alloys, a large isothermal magnetic entropy change across the first-order magnetostructural phase transition in an external magnetic field has been reported.[17,18,20,23,28,37]

In this work, we study the magnetic properties and the MCE of $Ni_{2+x}Mn_{1-x}Ga$ in the composition range $0.18 \leq x \leq 0.27$. We use the magnetic exchange parameters from first-principles calculations to obtain the magnetic phase diagram by means of MC simulations using the classical Heisenberg model (Sec. I). For the discussion of the MCE, we have used the q-state Potts model, which is coupled to the martensitic instability leading to a *coupled magnetostructural phase transition* for $0.18 \leq x \leq 0.27$. The Potts model is used here because it has advantages over the Heisenberg model regarding specific heat and entropy calculations at lower temperatures. The two structure models used in the Potts model MC simulations described in Secs. II and III, are the *simple cubic lattice model* denoted as model I (computationally fast) and the *full Heusler lattice model* denoted as model II (computationally more demanding). Model II allows a systematic search for magnetic Heusler systems with larger MCE.

II. FIRST-PRINCIPLES DESCRIPTION OF Ni-Mn-Ga ALLOYS

Figure 1 shows the cubic $L2_1$ ($c/a=1$) and tetragonal $L1_0$ ($c/a=1.25$) structure of $Ni_{2+x}Mn_{1-x}Ga$ and Fig. 2 shows the experimental phase diagram in the (x,T) plane for Ni-excess concentrations x.[35,38] The region of interest in the phase diagram where the MCE is important is confined to compositions $0.18 \leq x \leq 0.27$ with coinciding magnetic and structural transitions, i.e., there are only two phases: paramagnetic austenite with cubic $L2_1$ structure and ferromagnetic martensite with $L1_0$ structure. The structural transformation follows the tetragonal Bain transformation from $c/a=1$ ($L2_1$) to $c/a=1.25$ ($L1_0$) with very little volume change.

In order to check the transformation behavior, we have undertaken first-principles zero-temperature calculations employing the generalized gradient approximation (GGA),[39] projector-augmented wave approach,[40,41] and the Vienna *ab initio* Simulation Package (VASP);[41,42] an energy cutoff of 478 eV and 64 k points in the irreducible wedge of the Brillouin zone have been used.

The calculations of the energetic changes along the tetragonal deformation path, which transforms the unit cell in Fig. 1(a) to that in Fig. 1(b), are displayed in Fig. 3. The FM solution and two antiferromagnetic (AFM) solutions along the Bain path lie close in energy, where AFM involves antiferromagnetic alignment of Mn spins in two Mn-Ga layers separated by a Mn-Ga layer with ferromagnetic spin alignment. AFM-L denotes layer wise antiferromagnetic arrangement of Mn spins with complete spin reversal from layer to layer. Note that the tendency to build up AFM correlations as shown in Fig. 3, is related to environmental effects and slightly changing Mn-Mn distances and manifests itself in the exchange parameters by the appearance of AFM contributions in case of noncubic crystal structures, see Fig. 4.

In order to simulate in a simplified fashion the off-stoichiometric composition $x=0.25$ along the Bain transformation path, the Mn atom at centre position has been replaced by an extra Ni atom, which corresponds to $Ni_9Mn_3Ga_4$ (the nonstoichiomentric alloy with the same e/a would be $Ni_{2.25}Mn_{0.75}Ga$). The same unit cell was used by Banik *et al.*[43] in their structural studies of $Ni_{2+x}Mn_{1-x}Ga$.

Magnetic exchange parameters are helpful to complete the magnetic characterization of $Ni_{2+x}Mn_{1-x}Ga$. These have

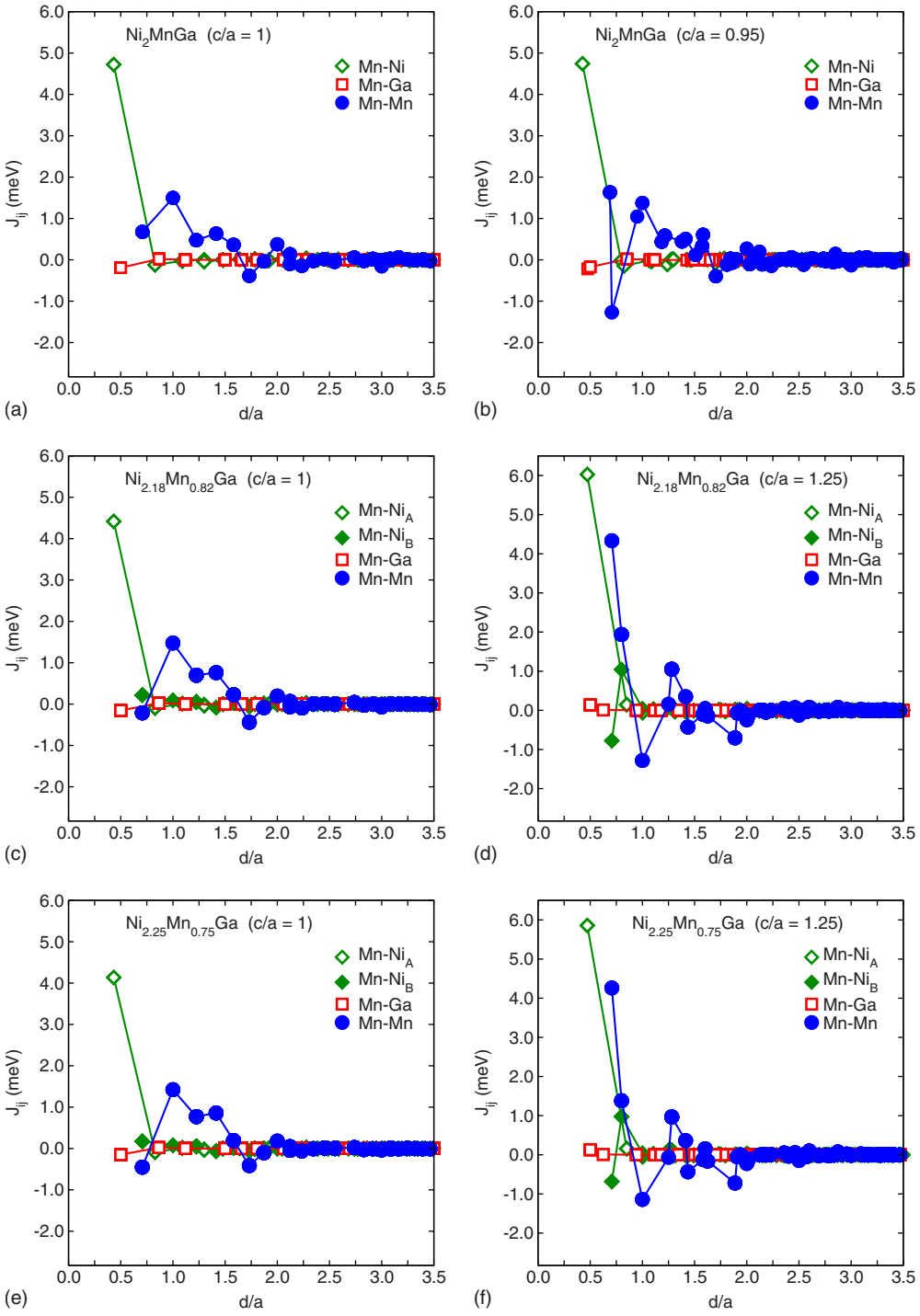

FIG. 4. (Color online) *Ab initio* magnetic exchange interactions of stoichiometric Ni_2MnGa with (a) $c/a=1$ (cubic), (b) $c/a=0.95$ (tetragonally distorted) and off-stoichiometric $Ni_{2.18}Mn_{0.82}Ga$ with (c) $c/a=1$ and (d) $c/a=1.25$ and $Ni_{2.25}Mn_{0.75}Ga$ with (e) $c/a=1$ and (f) $c/a=1.25$ as a function of the distance d/a between pairs of atoms i and j (in units of the lattice constant a). Mn-Mn, Mn-Ga, and Mn-Ni denote the corresponding J_{ij} between the atoms on their respective sublattices; the index A refers to Ni atoms on the Ni sublattice and index B to Ni atoms on the Mn sublattice, respectively. In each plot, a Mn atom is at the origin. When evaluating the J_{ij} for the nonstoichiometric cases in (c)–(f), the coherent potential approximation (CPA) and the SPR-KKR code (Ref. 46) have been used.

been calculated for the $L2_1$ and $L1_0$ structures and several x by employing Lichtenstein's formula[44,45] and the Munich SPR-KKR package[46] as well as the Machikaneyama code.[47] Using the local-density and scalar-relativistic approximation corresponding Curie temperatures obtained from MC simulations using the J_{ij} in the classical Heisenberg model are shown in the phase diagram in Fig. 2 by open circles. Regarding the J_{ij}, we note that the by far largest magnetic interaction occurs between the nearest-neighbor (nn) Mn and Ni_A atoms (Ni atoms on the regular Ni sublattice). This in-

teraction is ferromagnetic and mainly determines the magnitude of the Curie temperature T_C.

With increasing disorder and dilution of the magnetic lattice (i.e., with increasing x), the J_{ij} change systematically leading to lower T_C values, which agrees qualitatively with the experimental trend. However, the measured Curie temperature increases again with the onset of the magnetostructural transition at $x=0.18$, which is not displayed by the theoretical T_C values (open circles in Fig. 2). On the contrary, the Curie temperatures obtained from the Monte Carlo simulations using the *ab initio* J_{ij} as input parameters, lie below the extrapolated Curie temperatures T_C^A and T_C^M marked by dashed lines in Fig. 2. There may be several reasons for this.

(1) In the region of coinciding magnetic and structural phase transitions, local compositional changes may play an important role when determining the magnetic exchange parameters J_{ij}. Since we use Lichtenstein's formula[44,45] for small rotations of the spin moments with frozen potentials, which is good for ideal ferromagnetic systems, an additional averaging is required in case of atomic disorder so that

$$\langle J_{ij}\rangle_{\text{disorder}} = \left\langle \frac{1}{4\pi}\mathrm{Im}\int^{E_F} dE\ \mathrm{Tr}\{\Delta t_i(E) G_{ij}^{\uparrow}(E) \Delta t_j(E) G_{ij}^{\downarrow}(E)\} \right\rangle_{\text{disorder}}. \quad (1)$$

However, local variations are averaged out when using the single-site coherent potential approximation (CPA) which amounts to the replacement of each of the Green's functions in Eq. (1) by the corresponding CPA Green's function. Figure 4 shows only the results obtained in the single-site CPA and Fig. 2 shows the associated Curie temperatures. It is obvious that treatment, e.g., using the nonlocal CPA (see Ref. 48 and references therein) will be important, in particular, for compositions which exhibit the magnetostructural phase transition.

For other Heusler alloys such as Ni-Mn-(In, Sn, Sb) with even stronger antiferromagnetic correlations near the magnetostructural transition,[49,50] nonlocal CPA corrections will be important as well. A systematic investigation of nonlocal CPA effects on the J_{ij} in comparison with single-site CPA results is missing so far.

(2) When calculating the J_{ij}, the atomic sphere approximation and local-density approximation (LDA) within the Korringa-Kohn-Rostoker (KKR) CPA code have been used. We may expect a slight enhancement of the Mn spin moments and hence of T_C if instead of LDA, GGA, or full-potential calculations would have been used. These calculations are lengthy and have not been performed so far. The importance of full-potential calculations or rather a better treatment of electronic correlations has recently been highlighted for the half-metallic Heusler alloys.[51]

(3) Near the magnetostructural transition, an extreme sensitivity of the J_{ij} with respect to small abrupt changes in the volume at the phase transition can be expected, which is not taken into account in the calculation of the J_{ij}. Explicit inclusion of a magnetoelastic coupling term may help here which, however, is not really the subject of density-functional theory (DFT) calculations at zero temperature. The importance of the magnetoelastic interaction for the magnetostructural transition has recently been emphasized for $Ni_{50}Mn_{34.3}{}^{57}Fe_{0.5}In_{15.2}$ (Ref. 52) and $Ni_{50}Mn_{36.5}{}^{57}Fe_{0.5}Sn_{13}$.[53] Here, a *reverse* effect has been found, i.e., an abnormal magnetostructural transition due to weakening of exchange interactions caused by an abrupt change in the interatomic Mn-Mn distances at the transition, respectively. For the Ni-Mn-Ga alloys near the magnetostructural transition considered in this paper, an enhanced positive magnetoelastic coupling must be expected for $0.18 \leq x \leq 0.27$. The influence of the magnetic state on the structural transformation may also be important in non-Heusler systems such as elemental iron.[54]

(4) A further modification of the calculated T_C is expected if the change in the magnetic anisotropy energy (MAE) from the cubic to tetragonal structure with increasing x is considered. We have calculated the effect of increasing dilution of the magnetic sublattice on the MAE from Ni_2MnGa to $Ni_{2.25}Mn_{0.75}Ga$. For the latter alloy we obtain an MAE of ≈ 1.25 m Ry/f.u. with (001) as easy magnetization plane,[55] which would enhance T_C by a few kelvins, hence, not a big effect on T_C. This change in MAE is in agreement with previously reported results by Enkovaara *et al.*[56] and Gruner *et al.*,[55] (see also Sozinov *et al.*[57] and Heczko *et al.*[58]).

Such subtleties of magnetostructural phase transitions would require an exploration of DFT at finite temperatures which is beyond the scope of the present work. The model introduced below can handle such metamagnetic phenomena because of the extra magnetoelastic coupling term introduced in the model, which allows to adjust magnetic and structural phase transitions in such a manner that they coincide (*magnetostructural transition*). This highlights the importance of the magnetoelastic coupling in the magnetic Heusler alloys. Without such correlation, there will be no giant magnetocaloric effect.

In the following we will use the *ab initio* data for the discussion of the MCE in $Ni_{2+x}Mn_{1-x}Ga$ alloys. Two models are introduced: a simple cubic lattice model of interacting Mn spins and a realistic Heusler lattice model of interacting Mn and Ni spins. The first model originates from the observation that the Ni magnetic moments may be considered to be induced by the Mn moments and do not contribute with individual degrees of freedom to the temperature dependence of magnetization. Antiferromagnetic order of the Mn spins or the paramagnetic phase then necessarily implies vanishing Ni moments. In this case, we are left with a simple cubic lattice model of renormalized magnetic degrees of freedom which, in addition, are coupled to the lattice degrees of freedom for the description of the austenite-martensite transformation. A similar approach was successfully employed by Mryasov *et al.*[59] for the description of magnetic interactions in FePt using an effective Fe-Fe-spin model including a biquadratic spin interaction term. On the other hand, Ležaić *et al.*[60] have demonstrated for the half-metallic half-Heusler alloy NiMnSb that longitudinal fluctuations of the Ni moment are energetically as important as transversal, i.e., Heisenberg-type, ones. Furthermore, combined DFT and model calculations of the inverse magnetocaloric alloy α-FeRh predict that longitudinal fluctuations of the induced Rh moment (which takes over a role which is similar to the Ni moments in the

Heusler alloys) can provide a significant contribution to the large entropy change at the metamagnetic phase transition.[61] Thus, it may be questioned whether an effective Mn-Mn-spin model is really sufficient for all alloys. Therefore, we introduced the real Heusler structure with explicit spin degrees of freedom for Mn and Ni sites in order to account for the subtle differences between both descriptions. It turned out that indeed better results are obtained when retaining all possible magnetic exchange interactions when discussing entropic changes over the magnetostructural transition for the MCE. Nevertheless, we start with the simple cubic lattice model to introduce the underlying physics of the magnetostructural coupling.

III. MODEL I: COUPLING OF SPIN AND DISTORTION ON THE SIMPLE CUBIC LATTICE

For the description of magnetic ordering and structural transformations we make use of the q-state Potts model, which is supplemented by an Ising-type term for modeling tetragonal distortions. We have used the q-state Potts model (instead of the Heisenberg model) since the use of *discrete* spin variables guarantees the *well behavior* of magnetic entropy and specific heat over the whole temperature range.

In order to simplify the simulations and to decrease the computational efforts, we first consider the case of a simple cubic lattice with periodic boundary conditions taking into account only the nn interactions between effective atoms (neither Ni nor Mn but atoms which resemble Mn and have a large spin moment), which interact via a large positive J_{ij} with each other (model I). The J_{ij} are average values, which have been obtained from averaging the *ab initio* values over atomic shells.

Thus, stoichiometric Ni_2MnGa is described in the cubic lattice model by having all sites occupied by these effective Mn-like atoms. Off-stoichiometric $Ni_{2+x}Mn_{1-x}Ga$ alloys are described by binary "$Ni_{2+x}Mn_{1-x}$" alloys. Only the Mn-like atoms are assumed to have a magnetic moment, where the atoms may be displaced from their ideal cubic lattice sites (tetragonal distortion) while the Ni atoms have no magnetic moments and only a displacement degree of freedom. In view of the tiny Ni-spin moments, this is a reasonable assumption (magnetic Compton-scattering study of $Ni_{2+x}Mn_{1-x}Ga$ has shown that the small magnetic moment of the excess Ni atoms on the Mn sublattice remains essentially unchanged).[62]

The magnetic degrees of freedom are described by the q-state Potts model, which allows first-order and second-order transition from the ferromagnetic to the paramagnetic state depending on the interaction strength.[63] Here, q is the number of spin states, where $q=2$ is identical with the Ising model. For the effective Mn atom in the simple cubic lattice model, we use five spin states, since the spin moment S of the original Mn atoms is 4/2 allowing $2S+1$ spin projections $(-2,-1,0,1,2)$. Hence, the magnetic part of the Hamiltonian including an external magnetic field H_{ext} may be written as

$$\mathcal{H}_m = -\sum_{\langle ij\rangle} J_m(i,j)\,\delta_{S_i,S_j} - g\mu_B H_{ext}\sum_i \delta_{S_i,S_g}, \tag{2}$$

$$\delta_{S_i,S_g} = \begin{cases} 1 & S_i = 2 \\ 0 & \text{else}, \end{cases} \tag{3}$$

where $J_m(ij)$ is the magnetic exchange parameter, which may become negative depending on the degree of tetragonal distortion or disorder. The Kronecker symbol, δ_{S_i,S_j}, restricts the spin-spin interactions to the interactions between the same q states. The sum is performed over all nn spin pairs. In the simple cubic lattice model, $J_m(ij)$ is replaced by a constant (averaged) value J_m. The other Kronecker symbol, δ_{S_i,S_g}, couples the spin system via the $q=5$ (i.e., $S_i=2$) Potts state to the external magnetic field. S_g is called *ghost spin*,[64] its impact is that positive H_{ext} favors spins parallel to the *ghost spin*. μ_B is the Bohr magneton and g is the Landé factor.

In distinction to the Ising model, the magnetization of the q-state Potts model is obtained by

$$m = \frac{1}{L^3}\frac{qN_{max} - N_{mag}L^3}{q-1}, \tag{4}$$

where L is the linear dimension of the system ($L^3=N$), N_{max} the maximum number of identical magnetic states on the lattice, N_{mag} is the number of magnetic atoms, and q denotes the number of magnetic states at each lattice site.

In order to incorporate the mutual influence of magnetic ordering and structural transformation from cubic austenite to tetragonally distorted martensite with decreasing temperature, we make use of the degenerate Blume-Emery-Griffiths (BEG) model,[65] which allows one to describe the interaction between the elastic variables. This model contains the basic physical ingredients to describe martensitic transformations.[66,67]

In this model, the cubic austenite corresponds to a state with zero displacement ($\delta x=\delta y=\delta z=0$) whereas the martensite consists of structural variants with elongation and contraction along x, y, and z axes giving rise to six structural variants. In the present model, we retain only two of them, corresponding to distortions along one of the cubic axes, which leaves us with a high-temperature cubic phase of twofold degeneracy.

As discussed in Refs. 49 and 67, we introduce for each lattice site $i=1\ldots N$ a variable $\sigma_i=\pm 1,0$ defining the deformation state near each lattice site, with $\sigma_i=0$ as undistorted phase taken to be p-fold degenerate, which allows to approximately account for the high entropy of the lattice vibrations in the cubic phase.[67] The states $\sigma_i=\pm 1$ represent the distorted phase. The corresponding lattice Hamiltonian is essentially the one introduced by Castán *et al.*[67] supplemented by a term which favors the variant $\sigma_i=1$ in the presence of an external magnetic field,

$$\mathcal{H}_{lat} = -J\sum_{\langle ij\rangle}\sigma_i\sigma_j - K\sum_{\langle ij\rangle}(1-\sigma_i^2)(1-\sigma_j^2) - k_BT\ln(p)\sum_i(1-\sigma_i^2) - K_1 g\mu_B H_{ext}\sum_i \delta_{\sigma_i,\sigma_g}\sum_{\langle ij\rangle}\sigma_i\sigma_j. \tag{5}$$

The first term characterizes the interaction between σ_i and σ_j in tetragonal martensite while the second term defines the interaction between the σ_i in cubic austenite. Large values of K will stabilize the pure cubic phase for which $\sigma_i=0$ holds. For small values of K, an intermediate modulated (premartensitic) cubic phase may form having equal population of the strain variables $\sigma_i=\pm 1$ and $\sigma_i=0$.[67] Premartensite is not of interest here, since there is no intermediate state involved around the magnetostructural transition, which is the primary interest of this paper. K_1 is the dimensionless magnetoelastic interaction constant.

The term $k_BT\ln(p)$ may be regarded as a temperature-dependent crystal field which arises from the augmentation of the entropy of the cubic state ($\sigma_i=0$) by assigning it the degeneracy factor p (see also Ref. 68) regarding the equivalence of the p degenerate and ordinary Blume-Emery-Griffiths models. In Ref. 67 and also here, p is fixed to $p=2$. Finally, the parameter K in conjunction with the degeneracy factor p of the cubic phase, controls the order of the transition which changes from second (for small K) to first order (for large K). So, a large degeneracy p may initiate first-order premartensitic transitions.

The preference of one martensitic variant in an external magnetic field can be induced by coupling the strain variable σ_i to another *ghost variable*, σ_g, with the condition

$$\delta_{\sigma_i,\sigma_g}=\begin{cases}1 & \sigma_i=1\\ 0 & \text{else},\end{cases} \tag{6}$$

where σ_g may be considered as a *ghost deformation state*, characterized by the structural variant which is favored in the external magnetic field H_{ext}. A somewhat similar term has been used in Ref. 69 in a Landau functional theory of elastic and magnetic interactions.

Nonetheless, such a term allows to retain in a very easy way the experimental trend that the martensitic transformation temperature increases with increasing external magnetic field in Ni-Mn-Ga alloys because the magnetization in martensite is slightly stronger than in austenite (see also Refs. 70 and 71).

Two order parameters may be conceived,

$$\epsilon=\frac{1}{N}\sum_i \sigma_i, \tag{7}$$

$$\eta=\frac{1}{N}\sum_i \sigma_i^2, \tag{8}$$

where ϵ describes the degree of distortion, with $\epsilon=0$ as cubic phase with equal occurrence of $\sigma_i=\pm 1,0$, while η can be considered as modulation of the atoms in the lattice planes or shuffling of the atoms. As mentioned before, because we are interested in magnetostructural transitions where intermediate martensites are absent, the latter order parameter is not of interest (see Ref. 67 for a discussion of η involving first-order phase transitions from the cubic to the premartensitic phase).

For the coupling of magnetic and structural variables, Castán[67] has used the following symmetry allowed interactions,

$$\begin{aligned}\mathcal{H}_{int}=&-U_{00}\sum_{\langle ij\rangle}\delta_{S_i,S_j}(1-\sigma_i^2)(1-\sigma_j^2)\\&-U_{01}\sum_{\langle ij\rangle}\delta_{S_i,S_j}[\sigma_i^2(1-\sigma_j^2)+\sigma_j^2(1-\sigma_i^2)]\\&-U_{11}\sum_{\langle ij\rangle}\delta_{S_i,S_j}\sigma_i^2\sigma_j^2,\end{aligned} \tag{9}$$

where we have replaced the product of Ising variables, S_iS_j, used in Ref. 67 by the Potts' variables. The coupling constants $U_{\sigma,\sigma'}$ can, in principle, be obtained from *ab initio* calculations by studying various energy differences involving tetragonal lattice distortions in the vicinity of the martensitic transformation. However, for simplicity, we consider here as in Ref. 67 the case $U_{00}=U_{11}=0$ and set $U_{01}=-U$, which yields the simplified Hamiltonian,

$$\mathcal{H}_{int}=2U\sum_{\langle ij\rangle}\delta_{S_i,S_j}\left(\frac{1}{2}-\sigma_i^2\right)\left(\frac{1}{2}-\sigma_j^2\right)-\frac{1}{2}U\sum_{\langle ij\rangle}\delta_{S_i,S_j}, \tag{10}$$

where the first term describes the effective coupling (proportional to the square of the magnetization) to the modulation of the lattice while the last term renormalizes the spin-spin interaction.

The total Hamiltonian is then the sum of terms,

$$\mathcal{H}=\mathcal{H}_m+\mathcal{H}_{lat}+\mathcal{H}_{int}. \tag{11}$$

We would like to point out that the Hamiltonian in Eq. (11) has been used by Castán *et al.*[67] to discuss magnetic, premartensitic, and martensitic phase transitions in a qualitative manner, i.e., no *ab initio* input parameters; also the *ghost* variables as well as the direct coupling of the external magnetic field to a specific martensitic variant were omitted. Buchelnikov *et al.*[49] have used the full Hamiltonian plus an additional term accounting for the antiferromagnetic interactions appearing with the lattice distortion as well as parameters from *ab initio* calculations to study the unusual magnetic behavior of Ni-Mn-(In, Sn, Sb). This has shown that the model is rather powerful and may correctly describe the experimental phase diagrams.

In order to discuss the MCE of $Ni_{2+x}Mn_{1-x}Ga$ for compositions $0.18\leq x\leq 0.27$, we need to calculate further quantities such as the temperature dependence of the specific heat, $C=C_{mag}+C_{el}+C_{lat}$ with magnetic, electronic, and lattice contribution (C_{el} has been omitted throughout the paper), and entropy S_{mag} as well as the magnetic (χ_{mag}) and structural (χ_ϵ) susceptibility defined by

$$C_{mag}(T,H_{ext})=\frac{1}{k_BT^2}[\langle\mathcal{H}^2\rangle-\langle\mathcal{H}\rangle^2], \tag{12}$$

$$S_{mag}(\Delta T,H_{ext})=\int_{T_1}^{T_2}dT\frac{C_{mag}(T,H_{ext})}{T}, \tag{13}$$

$$\chi_{mag}(T,H_{ext})=\frac{1}{k_BT^2}[\langle m^2\rangle-\langle m\rangle^2], \tag{14}$$

$$\chi_\varepsilon(T,H_{ext}) = \frac{1}{k_B T^2}[\langle \epsilon^2 \rangle - \langle \epsilon \rangle^2]. \quad (15)$$

For the lattice heat capacity we will use the Debye approximation,

$$C_{lat}(T,\Theta_D) = 9RN_i\left\{4\left(\frac{T}{\Theta_D}\right)^3 \int_0^{\Theta_D/T} dx \frac{x^3}{e^x - 1} - \left(\frac{\Theta_D}{T}\right)\frac{1}{e^{\Theta_D/T}-1}\right\}, \quad (16)$$

where N_i is the number of ions per formula unit and Θ_D is the Debye temperature.

In order to calculate the isothermal entropy and adiabatic temperature changes with varying external magnetic field, we make use of

$$\Delta S_{mag}(T,H_{ext}) = S_{mag}(T,H_{ext}) - S_{mag}(T,0), \quad (17)$$

$$\Delta T(T,H_{ext}) = -T\frac{\Delta S_{mag}(T,H_{ext})}{C(T,H_{ext})}. \quad (18)$$

Here, $S_{mag}(T,H_{ext})$ and $S_{mag}(T,0)$ denote the entropy in presence of a magnetic field H_{ext} and in zero field, respectively. Note that in Eq. (18), $C(T,H_{ext})$ is the total specific heat of magnetic and lattice contribution.[72] Because $S_{lat}(T,H_{ext}) \approx S_{lat}(T,0)$, i.e., $\Delta S_{lat}(T,H_{ext}) \approx 0$, the adiabatic temperature change in Eq. (18) is the total temperature change available in magnetic refrigerants for temperatures near the magnetostructural transition slightly above room temperature. The hypothetical $\Delta T_{mag}(T,H_{ext})$ may be obtained from Eq. (18) if we replace $C(T,H_{ext})$ by $C_{mag}(T,H_{ext})$.

All quantities in Eqs. (11)–(18) can be evaluated from the MC simulations. Since we use Eq. (13) for the evaluation of the isothermal entropy change and do not use Maxwell relations (i.e., the *magnetic* analogue of the Clausius-Clapeyron equation), our procedure is more appropriate compared to the standard procedure used in most experimental work, where the magnetization curves for different magnetic fields are analyzed over the magnetic and martensitic phase transitions by

$$\Delta S_{mag}(T,H_{ext}) = S_{mag}(T,H_{ext}) - S_{mag}(T,0) = \mu_0 \int_0^{H_{ext}} dH_{ext}\left(\frac{\partial M}{\partial T}\right)_{H_{ext}}, \quad (19)$$

where μ_0 is the permeability of free space. In particular, Eq. (19) has been used in the context of *conventional* and *inverse* MCE in Ni-Mn-Sn and Ni-Mn-In alloys, respectively, where *conventional* and *inverse* effect may be distinguished by the sign of $(\partial M/\partial T)_{H_{ext}}$.[32,73,74]

A. Choice of parameters for model I

For the simple cubic lattice model, the calculation of magnetocaloric properties of $Ni_{2+x}Mn_{1-x}Ga$ has been performed by using the parameters listed in Table I with J_m taken as an average value over the exchange constants in Fig. 4 of the first three neighbor shells yielding a value of approximately 4 meV.[49] An approximate value for J may be estimated from the experimental phonon-dispersion curves of Ni-Mn-Ga alloys if J is assumed to be proportional to the soft phonon energy.[49,75,76] This yields 2 meV for the compound with T_C=364 and T_m=284 K. For K and U, which fix T_m, we have assumed both quantities to be positive (positive U is dictated by experiment because of the positive volume magnetostriction constant).[77] A negative magnetoelastic constant may exist near the premartensitic transition in Ni_2MnGa as calculations for a two-dimensional lattice model have shown.[67] However, premartensitic phenomena do not exist in the region $0.18 \le x \le 0.27$.

TABLE I. Parameters (in meV) used in the simple cubic lattice model for the $Ni_{2+x}Mn_{1-x}Ga$ alloys (K_1 is taken to be 0.4 for each composition).

Nickel excess (x)	0.18	0.20	0.22	0.24	0.27
J_m	4.0	4.2	4.48	4.403	4.155
J	2.42	2.485	2.58	2.56	2.43
K	1.016	0.994	0.968	0.896	0.729
U	0.121	0.298	0.516	0.998	1.8

Although values for K may be obtained from *ab initio* simulations, we use here a simpler procedure. In general, for $K/J > 0.5$, we obtain three consecutive phase transitions with decreasing T: a magnetic transition from the paramagnetic to the ferromagnetic phase at T_C, a premartensitic transition from the cubic to the quasicubic phase at T_P, and a martensitic transition from the quasicubic to the tetragonal phase T_m with $T_m < T_P < T_C$.[67] For the compositions $0.18 \le x \le 0.27$, we may get rid of the premartensitic phase by choosing $K/J < 0.5$.

The final values of K and U in Table I have been chosen such that for a given ferromagnetic exchange parameter J_m, the magnetic and structural phase transition temperatures coincide. $K_1 \approx 0.4$ assures that both transition temperatures still coincide in the presence of an external magnetic field too.

Instead of fixing J by the soft phonon energy of 2 meV, we have used as in Ref. 49 a slightly different procedure by introducing reduced temperatures T^* and T^*_{ms},

$$T^* = k_B T/zJ, \quad T^*_{ms} = k_B T_{ms}/zJ, \quad (20)$$

where T_{ms} is the magnetostructural transition temperature and z=6 is the number of nn of the simple cubic lattice. This sets $k_B T_{ms}$ in relation to J, which may be used to let magnetic and structural phase transitions merge together as demonstrated for Ni-Mn-X (X=In,Sn,Sb).[49] For $Ni_{2+x}Mn_{1-x}Ga$ considered here, the magnetostructural phase transition is approximately fixed by T^*_{ms}=2. Taking this value, the structural parameter J for $Ni_{2.18}Mn_{0.82}Ga$ with $T_{ms} \approx 338$ K (Ref. 37) is $J \approx 2.42$ meV, being slightly different from 2 meV estimated from the soft phonon energy. In the MC simulations, we have used the values of Table I obtained in such a way.

Since the elastic properties of Ni-Mn-Ga change with temperature, all model parameters also depend on tempera-

ture. In principle, the magnetic exchange parameters and elastic energy parameters could be calculated by *ab initio* method using the finite-temperature lattice parameters from experiment. However, this would require large numerical efforts. Here, we will assume that this temperature dependence may be safely neglected.

B. Computational results for model I

The MC simulations have been carried out employing the standard Metropolis algorithm[78] for the simple cubic lattice model and compositions $x=0.18$, 0.20, 0.22, 0.24, and 0.27. Changes in the independent variables q and σ_i are accepted or rejected according to a single-site transition probability $W=\min\{1,\exp(-\Delta\mathcal{H}/k_BT)\}$. The number of sites used in the simulations was $N=15^3$, where the configuration of Ni-excess atoms on the Mn sublattice was chosen randomly. One Monte Carlo step consists of N attempts to change the variables q and σ_i meaning that for a given temperature, the number of Monte Carlo steps on each site varied from 10^5 to 10^6. We started the simulations in the ferromagnetic martensitic phase with $q=2$ and $\sigma_i=1$. The energy $\mathcal{H}$ of the system and the order parameters m and ϵ were averaged over 400 configurations for each 100 Monte Carlo steps. In order to obtain equilibrium values of $\mathcal{H}$, m, and ϵ, the first 10^4 Monte Carlo steps were discarded. The degeneracy factor p and the Landé factor g were taken as $p=2$ and $g=2$. The multiplicity of spin state, i.e., q, was chosen as a random number r with $0<r<1$ by fixing q according to the scheme: If $0\le r\le l/5$ then $q=l$, $l=1,\ldots,5$.

The temperature dependence of the normalized magnetization, tetragonal distortion, and susceptibility of the magnetic and strain order parameters are shown in Fig. 5 for the composition $Ni_{2.18}Mn_{0.82}Ga$. The merging of magnetic and martensitic phase transitions is clearly visible from the coinciding peaks of magnetic (χ_{mag}) and strain (χ_ϵ) susceptibility shown in the upper part of Fig. 5. Furthermore, Fig. 5 reveals that the magnetostructural phase transition temperature increases by ≈ 6 K with increasing external magnetic field H_{ext} from 0 to 5 T, which is in agreement with the experimentally observed shift of ≈ 1 K/T.[79]

Theoretical and experimental results for the temperature variation in the magnetization for different compositions in a magnetic field of 5 T are presented in Fig. 6. The theoretical magnetization M (in units of Gauss) was obtained from $M=mM_0$, where m is normalized magnetization and M_0 is the saturation magnetization for stoichiometric Ni_2MnGa derived from

$$M_0 = \frac{R\rho g\mu_B S}{\mu k_B}, \tag{21}$$

where R is the gas constant, S the spin moment, ρ the density of the alloy, μ_B is Bohr's magneton, g the Landé factor, k_B the Boltzmann constant, and μ is the molar mass. For Ni_2MnGa we have taken the following values: $g=2$, $S=4/2$, $\rho=8.1$ g/cm^3, and $\mu=242$ g/mol. It is obvious from Fig. 6 that the magnetization decreases with increasing Ni excess due to the dilution of the magnetic subsystem.

Figure 7 shows the composition dependence of magnetic and strain susceptibility of $Ni_{2+x}Mn_{1-x}Ga$ alloys as a function

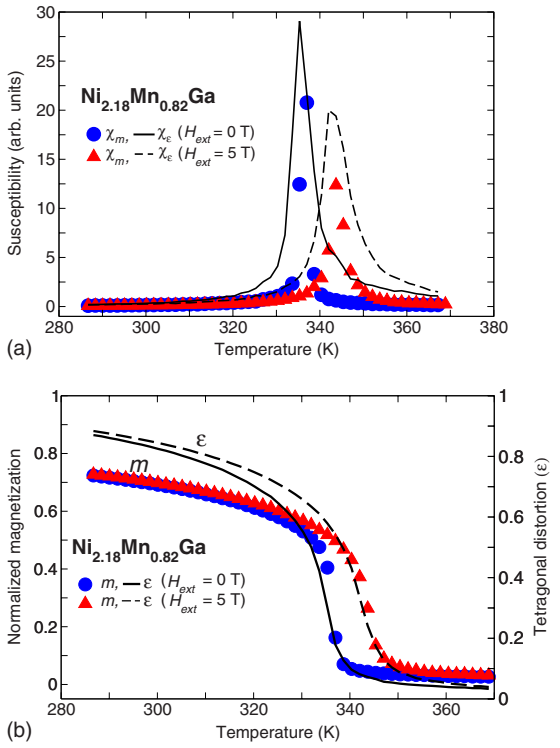

FIG. 5. (Color online) Results of MC simulations using model I showing (a) the temperature dependence of the magnetic susceptibility [filled circles (blue): $\chi_{mag}(T,H_{ext}=0$ T) and filled triangles (red): $\chi_{mag}(T,H_{ext}=5$ T)] and strain susceptibility [solid lines: $\chi_\epsilon(T,H_{ext}=0$ T) and dashed lines: $\chi_\epsilon(T,H_{ext}=5$ T)] of $Ni_{2.18}Mn_{0.82}Ga$; (b) the temperature dependence of normalized magnetization m and tetragonal distortion ϵ in 0 T and 5 T, respectively; same symbols as in (a).

of temperature in zero external magnetic field indicating that for each composition, the peaks of both susceptibility curves coincide, defining the magnetostructural transition, in agreement with the experimental phase diagram[35] in Fig. 2. The calculated temperature dependence of the magnetic contribution to the specific heat in zero magnetic field is shown in Fig. 8. We notice a decrease in the magnitude of the magnetic specific heat with increasing Ni-excess atoms.

Comparison of the computational results for the specific heat with available experimental data for the compositions $x=0.18$, 0.19, and 0.24, leads to the following observation: The change in specific heat at the T_{ms} of $Ni_{2.18}Mn_{0.82}Ga$,[80] $Ni_{2.19}Mn_{0.81}Ga$,[81] and $Ni_{2.24}Mn_{0.76}Ga$ (Ref. 80) is approximately obtained as 153 J/(mol K), 145 J/(mol K), and 132 J/(mol K), respectively. Our theoretical values for the specific heat change at the T_{ms} of $Ni_{2.18}Mn_{0.82}Ga$ and $Ni_{2.24}Mn_{0.76}Ga$ are 285 J/(mol K) and 180 J/(mol K), respectively, showing that the underlying simple model used in the simulations yields reasonable results because of the rather good fitting of the model parameters: J_m from *ab initio* and J from fixing T_{ms}.

Figure 9 shows the calculated entropy variation in $Ni_{2.18}Mn_{0.82}Ga$ for various magnetic fields, $H_{ext}=0$, 1.85, and 5 T, using Eq. (13) with $T_1=290$ and $T_2=375$ K. We would like to remind again that Monte Carlo simulations of the classical Heisenberg Hamiltonian do not reproduce the satu-

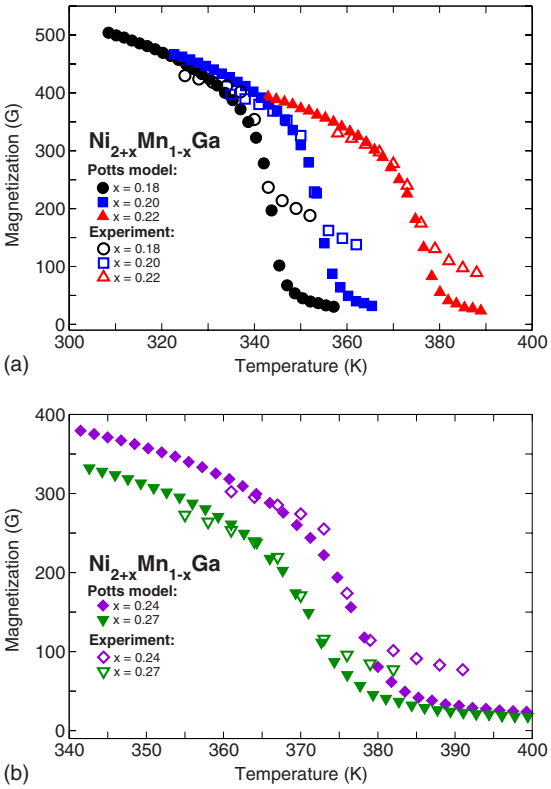

FIG. 6. (Color online) Monte Carlo results using model I (filled symbols) compared to experimental results (open symbols) of magnetization curves of $Ni_{2+x}Mn_{1-x}Ga$ alloys in an external magnetic field of 5 T. The experimental results were taken from Ref. 37. Figure (a) shows the results for $Ni_{2.18}Mn_{0.82}Ga$, $Ni_{2.20}Mn_{0.80}Ga$, and $Ni_{2.22}Mn_{0.78}Ga$ while figure (b) those for $Ni_{2.24}Mn_{0.76}Ga$ and $Ni_{2.27}Mn_{0.73}Ga$, respectively.

ration value of the magnetic entropy, $S_{mag}=R\ln(2S+1)$, where $2S+1$ is the number of available spin states, because the spins are treated as classical variables, which may take on continuous values. Thus, in order to obtain the first-order magnetic phase transition and reproduce the expected saturation value of the magnetic entropy we have used the q-state Potts model, for which the z components of the spin can take discrete values in the interval $-4/2 \leq S_{iz} \leq 4/2$. Taking into account that in the cubic phase the entropy of our model is determined by the magnetic subsystem only, the calculated saturation value of the entropy of $S_{mag} \approx 12$ J/(mol K) is almost consistent with the expected one [≈13.3 J/(mol K)] given by $S_{mag}=R\ln(2S+1)$. Figure 9 also shows that the entropy in zero magnetic field exhibits a break around $T \approx 338$ K, which is indicative for first-order phase transition characteristics of T_{ms}.

In Fig. 10, we present the isothermal magnetic entropy change ΔS_{mag} in $Ni_{2.18}Mn_{0.82}Ga$ for different magnetic fields ranging from 0 to 1.85 T assuming that the structural part of the entropy does not change significantly with the magnetic field. The experimental results for ΔS_{mag} were obtained from isothermal magnetization measurements with the help of the Maxwell relation.[37] It is obvious that the theoretical curve of the isothermal magnetic entropy change is in good agreement with the experimental data.

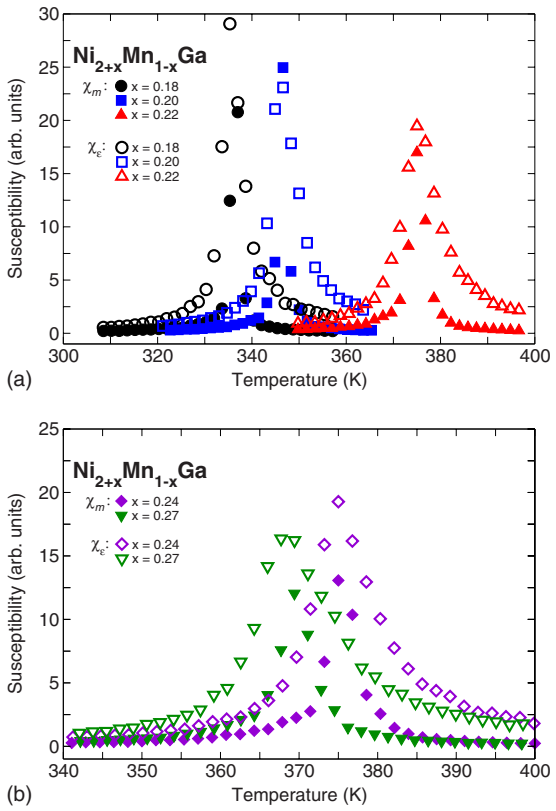

FIG. 7. (Color online) Monte Carlo results using model I showing the magnetic (filled symbols) and strain (open symbols) susceptibility as a function of temperature for $Ni_{2+x}Mn_{1-x}Ga$ alloys in zero magnetic field. Figure (a) shows the results for $Ni_{2.18}Mn_{0.82}Ga$, $Ni_{2.20}Mn_{0.80}Ga$, and $Ni_{2.22}Mn_{0.78}Ga$ while figure (b) displays the results for $Ni_{2.24}Mn_{0.76}Ga$ and $Ni_{2.27}Mn_{0.73}Ga$, respectively. For each composition, the coinciding peaks of χ_m and χ_ϵ curves identify the magnetostructural phase transition temperature T_{ms}.

Using the temperature variation in the entropy for $H_{ext}=0$ T and $H_{ext}=5$ T, we calculated the isothermal magnetic entropy change for other $Ni_{2+x}Mn_{1-x}Ga$ alloys using

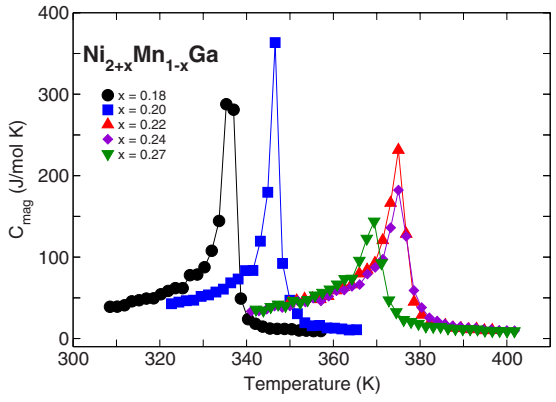

FIG. 8. (Color online) Monte Carlo simulations using model I of the temperature dependence of the magnetic contribution to the zero-field specific heat of $Ni_{2+x}Mn_{1-x}Ga$ alloys for $x=0.18$, 0.20, 0.22, 0.24, and 0.27, respectively. For each composition, the peaks in the specific-heat curves mark the magnetostructural phase transition.

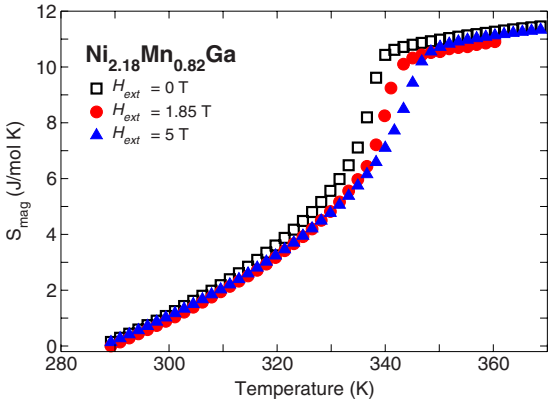

FIG. 9. (Color online) Monte Carlo simulations using model I of the temperature dependence of the magnetic entropy of $Ni_{2.18}Mn_{0.82}Ga$ in magnetic fields H_{ext}=0 T, 1.85 T, and 5 T, respectively. The curves have been obtained by integrating corresponding specific-heat curves using Eq. (13).

Eqs. (13) and (17). The resulting temperature dependence of ΔS_{mag} in magnetic fields from 0 to 5 T shows that $Ni_{2.18}Mn_{0.82}Ga$ and $Ni_{2.20}Mn_{0.80}Ga$ have maximum values of ΔS_{mag} and that the isothermal magnetic entropy change decreases with further increasing the Ni-excess concentration x, see Fig. 11. The discrepancy between the peak value of ΔS_{mag} calculated by the Monte Carlo method and the one determined from the isothermal magnetization curves with the help of the Maxwell relation, may be due to limited applicability of the Maxwell relation to materials undergoing first-order magnetic phase transitions and due to the simple cubic lattice model. To summarize, the magnetocaloric properties of model I have been collected in Table II.

IV. MODEL II: COUPLING OF SPIN AND DISTORTION ON THE FULL HEUSLER LATTICE

In this section we use the real three-dimensional lattice with periodic boundary conditions for Ni-Mn-Ga Heusler alloys. The unit cell arises from four interpenetrating fcc sublattices, see Fig. 1(a). This unit cell corresponds to the high-temperature cubic phase in which lattice distortions are absent. During cooling the austenitic phase transforms to the low-temperature tetragonal martensite, see Fig. 1(b). As discussed before, the martensitic phase consists of six variants which may be described by lattice distortions, from which we retain only two variants.

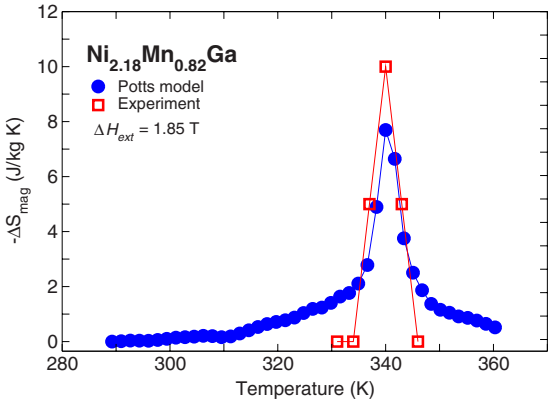

FIG. 10. (Color online) Monte Carlo simulation using model I of the isothermal magnetic entropy change ΔS_{mag} in $Ni_{2.18}Mn_{0.82}Ga$ with varying magnetic field from 0 to 1.85 T obtained by using Eqs. (13) and (17) (filled circles) compared to experimental data (open squares) taken from Ref. 37.

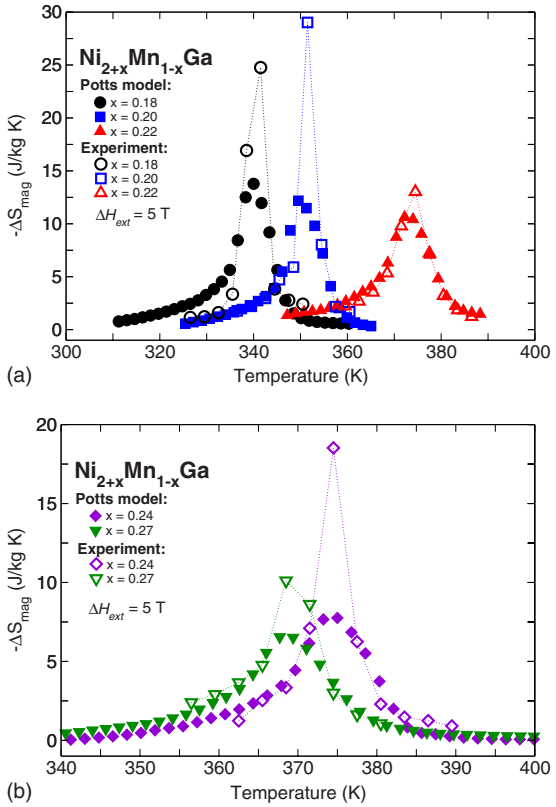

FIG. 11. (Color online) Results of Monte Carlo simulations using model I (filled symbols) versus experimental (open symbols) curves of the isothermal magnetic entropy change ΔS_{mag} of $Ni_{2+x}Mn_{1-x}Ga$ alloys in external magnetic fields from 0 to 5 T. The experimental results were taken from Ref. 37. Figure (a) shows the data for $Ni_{2.18}Mn_{0.82}Ga$, $Ni_{2.20}Mn_{0.80}Ga$, and $Ni_{2.22}Mn_{0.78}Ga$ while figure (b) shows the data for $Ni_{2.24}Mn_{0.76}Ga$ and $Ni_{2.27}Mn_{0.73}Ga$.

TABLE II. Model I: calculated values of heat capacities in J/(mol K) and MCE [ΔS_{mag} in J/(mol K), ΔT_{mag} and ΔT in K] for $Ni_{2+x}Mn_{1-x}Ga$ alloys upon variation in the magnetic field from 0 to 5 T obtained for the simple cubic lattice model. ΔT_{mag} is obtained from Eq. (18) when replacing the full specific heat $C(T,H_{ext})$ by only the magnetic contribution $C_{mag}(T,H_{ext})$.

Nickel excess (x)	0.18	0.20	0.22	0.24	0.27
C_{mag}	287.7	362	231.5	182.3	143.8
C	386.7	461	330.5	281.3	242.8
ΔS_{mag}	−3.33	−2.95	−2.56	−1.87	−1.58
ΔT_{mag}	3.39	2.85	4.15	3.85	4.03
ΔT	2.93	2.24	2.90	2.49	2.39

TABLE III. Nearest-neighbor magnetic exchange interactions J_{ij} in meV of some cubic and tetragonal $Ni_{2+x}Mn_{1-x}Ga$ Heusler systems. Ni_A refers to Ni atoms on the original Ni sublattice, Ni_B to Ni atoms on the Mn sublattice. Mn-Mn^{AF} refers to the antiferromagnetic exchange interaction which appears between nn Mn atoms on the regular and original sublattice, respectively (c.f. Fig. 4).

J_{ij}	$x=0$	$x=0.18$	$x=0.25$
	$(c/a=1.0)$		
$(d/a\approx 0.7)$ Mn-Mn	0.71	−0.02	−0.04
$(d/a\approx 0.47)$ Mn-Ni	4.85		
$(d/a\approx 0.47)$ Mn-Ni_A	1.63	4.6	4.26
$(d/a\approx 0.7)$ Mn-Ni_B		0.2	0.016
	$(c/a=0.95)$		
$(d/a\approx 0.69)$ Mn-Mn	1.63		
$(d/a\approx 0.7)$ Mn-Mn^{AF}	−1.3		
$(d/a\approx 0.47)$ Mn-Ni	4.9		
	$(c/a=1.25)$		
$(d/a\approx 0.7)$ Mn-Mn		4.33	4.26
$(d/a\approx 0.8)$ Mn-Mn		1.93	1.38
$(d/a=1.0)$ Mn-Mn^{AF}		−1.28	−1.14
$(d/a\approx 0.47)$ Mn-Ni_A		6.027	5.86
$(d/a\approx 0.7)$ Mn-Ni_B^{AF}		−0.77	−0.68
$(d/a\approx 0.8)$ Mn-Ni_B		1.039	0.97

In the off-stoichiometric alloys, the Ni-excess atoms occupy regular Mn positions, which in our model will be denoted as Ni_B in contrast to Ni_A atoms on the regular Ni sublattice. In stoichiometric Ni_2MnGa, the magnetic moment of $\approx 4\mu_B$ is largely confined to the Mn atoms; the contribution of the Ni atoms to the total magnetic moment is much smaller [$\approx 0.3\ \mu_B$/atom (Ref. 33)], and the contribution from the Ga atoms is practically negligible. As already noticed, the *ab initio* calculations of the magnetic exchange parameters show that the Mn-Ni_A exchange interaction is positive and by far the largest of all exchange integrals, which guarantees a ferromagnetic ground state. The J_{ij} presented in Fig. 4 show that in case of tetragonal phases ($c/a=0.95$ in case of Ni_2MnGa and $c/a=1.25$ in case of $Ni_{2.18}Mn_{0.82}Ga$ and $Ni_{2.25}Mn_{0.75}Ga$), the second-nearest Mn atoms interact antiferromagnetically. In the cubic phase, these antiferromagnetic interactions vanish. In the MC simulations of the full Heusler lattice model this different behavior of the J_{ij} is taken care of. The corresponding magnetic exchange parameters are listed in Table III (see also Fig. 4). Ni_A and Ni_B atoms are now assumed to have magnetic and structural degrees of freedom whereas sites occupied by Ga atoms have only structural degrees of freedom. Hence, the whole system can again be considered as consisting of interacting magnetic and structural subsystems which may be described by the same Hamiltonian (11).

For the Heusler lattice model, the magnetic degrees of freedom are now described by a slightly modified q-state Potts model which allows first- and second-order phase transitions.[63] Note that in experiment most paramagnetic-ferromagnetic phase transitions in the austenitic phase show a sudden increase in the magnetization since the magnetic field is usually not large enough to measure the saturation magnetization but the transitions are of second order.

Since the Ni-Mn interaction plays a dominant role regarding the stabilization of ferromagnetic order, we now take into account the spin moments S of both Mn and Ni atoms with $S=4/2$ and $2S+1$ spin projections (−2, −1, 0, 1, and 2) for the Mn atoms, i.e., $q_{\mathrm{Mn}}=5$, and $S=1$ with spin projections (−1, 0, and 1) and $q_{\mathrm{Ni}}=3$ for the Ni atoms. Therefore, we do the Monte Carlo simulations for a 3-5-state *Potts model*.

The structural part of the Hamiltonian is described as before by the degenerate 3-state BEG model allowing for the structural transformation from cubic austenite phase to tetragonal martensite.[67] Formally, the Hamiltonian is again given by Eq. (11), only that now we deal with a more realistic description of the Ni spin and use the real crystal lattice shown in Fig. 1.

In order to calculate the average energy at a given temperature, we practically use the same procedure as was employed in the simple cubic lattice case.

(1) We generate an initial spin and strain configuration in the ferromagnetically ordered state and choose the equilibrium strain configuration of the tetragonal or cubic lattice. For a particular site i and $\sigma_i=\pm 1$, the initial elastic energy $\mathcal{H}_{lat,1}$ is calculated according to Eq. (5) for the tetragonal lattice; if $\sigma_i=0$, the initial elastic energy $\mathcal{H}_{lat,1}$ is calculated for the cubic lattice.

(2) We then change randomly the value of strain σ_i and calculate for the new configuration $\mathcal{H}_{lat,2}$ according to the cases $\sigma_i=\pm 1$ and $\sigma_i=0$. If $\mathcal{H}_{lat,2}<\mathcal{H}_{lat,1}$, $\mathcal{H}_{lat,2}$ is accepted and we proceed further with step (3). If $\mathcal{H}_{lat,2}>\mathcal{H}_{lat,1}$, we calculate $\exp(-\Delta\mathcal{H}_{lat}/k_BT)$ and generate a random number r such that $0<r<1$; if $r<\exp(-\Delta\mathcal{H}_{lat}/k_BT)$, the new configuration with energy $\mathcal{H}_{lat,2}$ is accepted, else the old strain configuration is preserved and we proceed to step (3).

(3) Choose a spin configuration for the cubic or tetragonal lattice and calculate the energy $\mathcal{H}$ for the selected strain at site i by using Eq. (11). In case of $\sigma_i=\pm 1$ ($\sigma_i=0$), the tetragonal (cubic) lattice is used to calculate $\mathcal{H}_1$. If a tetragonal lattice is considered in Eq. (1), the antiferromagnetic interaction between second nn (snn) Mn atoms must be taken into account. We then change randomly the spin state q at site i and calculate the energy for this new configuration ($\mathcal{H}_2$) analogously to the evaluation of $\mathcal{H}_1$.

(4) We move to the next lattice site and repeat the procedure until all lattice sites have been swept. The whole process of the partition of the lattice is described by one Monte Carlo step.

For a given temperature, the average energy $\langle\mathcal{H}\rangle$ and average squared energy $\langle\mathcal{H}^2\rangle$ are calculated by using

$$\langle\mathcal{H}\rangle=\frac{1}{N_c-N_0}\sum_{i>N_0}^{N_c}\mathcal{H}_i,$$

$$\langle\mathcal{H}^2\rangle=\frac{1}{N_c-N_0}\sum_{i>N_0}^{N_c}\mathcal{H}_i^2, \tag{22}$$

where N_c is the total number of Monte Carlo steps, N_0 the number of Monte Carlo steps which are used for thermaliza-

TABLE IV. Model II: parameters (in meV) used in the real lattice model for the $Ni_{2.18}Mn_{0.82}Ga$ alloy.

Parameter	$c/a=1$	$c/a=1.25$
$(d/a\approx 0.7)$ $J_{\text{Mn-Mn}}$	−0.02	4.33
$(d/a\approx 0.8)$ $J_{\text{Mn-Mn}}$		1.93
$(d/a=1.0)$ $J_{\text{Mn-Mn}}$	1.47	−1.28
$(d/a\approx 0.47)$ $J_{\text{Mn-Ni}_A}$	4.64	6.027
$(d/a\approx 0.7)$ $J_{\text{Mn-Ni}_B}$	0.2	−0.77
$(d/a\approx 0.8)$ $J_{\text{Mn-Ni}_B}$		1.039
J	2.0	2.0
U	2.9	4.3
K	0.25	0.25

tion; the index i denotes the Monte Carlo step.

The magnetization of the 3-5-state Potts model is defined as

$$m=\frac{1}{N}\left(\frac{q_{\text{Ni}}N_{max}^{\text{Ni}}-N_{\text{Ni}}}{q_{\text{Ni}}-1}+\frac{q_{\text{Mn}}N_{max}^{\text{Mn}}-N_{\text{Mn}}}{q_{\text{Mn}}-1}\right), \tag{23}$$

where N is the total number of Ni and Mn atoms, q_{Ni} and q_{Mn} are the numbers of magnetic states of Ni and Mn atoms, N_{max}^{Ni} and N_{max}^{Mn} are the maximum numbers of identical magnetic states on the lattice and N_{Ni} and N_{Mn} are the numbers of Ni and Mn atoms on the lattice, respectively.

A. Choice of parameters for model II

For the calculation of magnetic and magnetocaloric properties of $Ni_{2.18}Mn_{0.82}Ga$, we have used the numerical parameters listed in Table IV (taken from the second column in Table III). As for model I, additional information is required to fix the actual parameter associated with the structural change which may be estimated as before from the phonon-dispersion curves of Ni-Mn-Ga alloys,[75,76] i.e., $J\approx 2$ meV at the structural phase transition temperature ($T_m=284$ K, $T_C=364$ K).

The values of magnetic exchange interactions between Mn-Mn, Mn-Ni_A, and Mn-Ni_B for cubic and tetragonal lattices are taken from the *ab initio* calculations of $Ni_{2.18}Mn_{0.82}Ga$. The antiferromagnetic interaction appearing in case of tetragonal distortion and disorder denoted by $J_{\text{Mn-Mn}}^{\text{AF}}$ and $J_{\text{Mn-Ni}_B}^{\text{AF}}$ in Table III enters Eq. (1) and is taken care of in the simulations.

Values for K, which fix the martensitic transition, and magnetoelastic interaction U have been determined for both martensite and austenite phases using the condition $U(c/a=1.25)>0$, $U(c/a=1)>0$, and $K>0$. As before, the choice of a positive sign for $U(c/a=1.25)$ and $U(c/a=1)$ is due to the positive sign of the volume magnetostriction in Ni-Mn-Ga.[77] Furthermore, we fix K and U as before by choosing $K/J<0.5$ for $Ni_{2.18}Mn_{0.82}Ga$; the values of $U(c/a=1.25)$, $U(c/a=1)$, and K given in Table IV were then chosen such that for fixed ferromagnetic exchange constants $J_{\text{Mn-Ni}_A}$, $J_{\text{Mn-Ni}_B}$, $J_{\text{Mn-Mn}}$, $J_{\text{Mn-Mn}}^{\text{AF}}$, and $J_{\text{Mn-Ni}_B}^{\text{AF}}$, we have coinciding magnetic and structural phase transitions. As for model I, the magnetoelastic interaction constant K_1 for $Ni_{2.18}Mn_{0.82}Ga$ is fixed such that the magnetic and the structural phase transition temperatures also coincide in the presence of external magnetic fields. This is achieved for $K_1\approx 0.25$. Also for this more refined full Heusler lattice model, the parameters still depend on temperature, which for the sake of simplicity has been ignored.

B. Computational results for model II

We now discuss results of MC simulations of $Ni_{2.18}Mn_{0.82}Ga$ using the full Heusler lattice model and the standard Metropolis algorithm.[78] Changes in the independent variables q_{Ni}, q_{Mn}, and σ_i are accepted or rejected according to a single-site transition probability $W=\min\{1,\exp(-\Delta\mathcal{H}/k_BT)\}$. Since the crystal lattice of the full Heusler alloys is used in the simulations, the coordination number of nn atoms takes on various values for each atom in the cubic and tetragonal lattices. For the magnetic subsystem in cubic austenite, each Mn atom has 12 nn Mn atoms, 8 nn Ni atoms and each Ni atom has 4 nn Mn atoms; in martensite, each Mn atom has 38 nn Mn and Ni atoms and 4 snn Mn atoms with which the considered Mn atom interacts antiferromagnetically, and each Ni atom has 4 nn Mn atoms. Regarding the structural subsystem in austenite, each atom Mn (Ga) has 12 nn Mn (Ga) atoms, 6 nn Ga (Mn) atoms, and 8 nn Ni atoms and each Ni atom has 4 nn Mn, Ga atoms and 6 nn Ni atoms; in martensite, each Mn (Ga) atom has 8 nn Mn (Ga) atoms, 2 nn Ga (Mn) atoms, and 8 nn Ni atoms, respectively, and each Ni atom has 4 nn Mn and Ga atoms and 6 nn Ni atoms.

The number of sites used in the simulation is $N=L^3$, where L is the number of cubic unit cells of Fig. 1(a), here, $L=6$. Thus we have used a lattice containing 900 Mn, 1728 Ni_A, 198 Ni_B, and 1099 Ga atoms. The configuration of Ni_B atoms on the Mn sublattice is set randomly and its total number is fixed by the composition of $Ni_{2.18}Mn_{0.82}Ga$. As time unit, we have used one Monte Carlo step consisting of N attempts to change the variables q_{Ni}, q_{Mn}, and σ_i. For a given temperature, we have used 5×10^5 Monte Carlo steps. The simulation was started in the ferromagnetic martensitic phase with $q_{\text{Ni}}=1$, $q_{\text{Mn}}=1$, and $\sigma_i=1$. The internal energy of the system $\mathcal{H}$ and the order parameters m and ϵ were averaged over 400 configurations for each 100 Monte Carlo steps. In order to obtain equilibrium values of $\mathcal{H}$, m, and ϵ, the first 10^4 Monte Carlo steps were discarded. As before, degeneracy factor p and Landé factor g were taken to be $p=2$ and $g=2$. The magnitude of spin states (i.e., q_{Ni} and q_{Mn}) was chosen as a random number r such that $0<r<1$, q_{Ni} and q_{Mn} were fixed according to the scheme: if $0\le r\le l/3$, $q_{\text{Ni}}=l$, $l=1\ldots 3$ and $0\le r\le l/5$, then $q_{\text{Mn}}=l$, $l=1,\ldots,5$.

Results of Monte Carlo simulations of the magnetic and magnetocaloric properties of $Ni_{2.18}Mn_{0.82}Ga$ are presented in Figs. 12–16. Figure 12 shows the simulated temperature variation in the magnetization and tetragonal distortion and the magnetic and strain susceptibility. Due to the choice of model parameters, the curves of the magnetic order parameter m and strain order parameter ϵ coincide in the phase

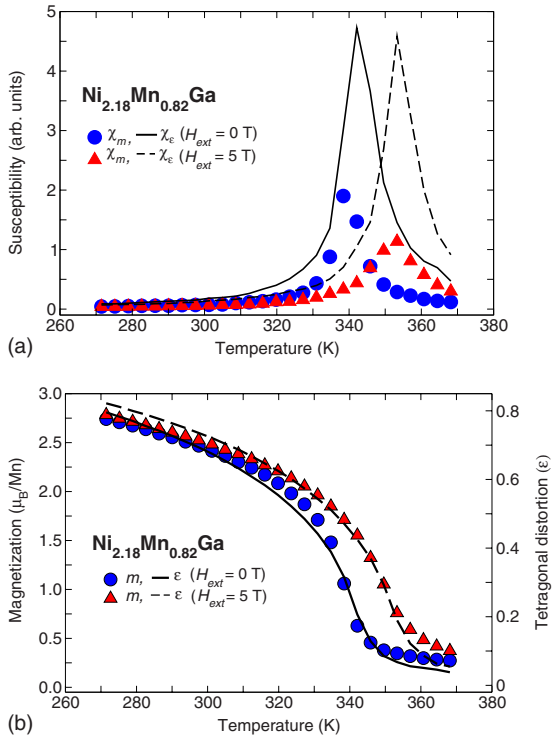

FIG. 12. (Color online) Monte Carlo results using model II showing (a) the temperature variation in magnetic (χ_{mag}) and strain (χ_ϵ) susceptibility of $Ni_{2.18}Mn_{0.82}Ga$ in magnetic fields of 0 T and 5 T, respectively, and (b) the temperature variation in magnetization m and tetragonal distortion ϵ in magnetic fields of 0 T and 5 T, respectively. Same symbols as in Fig. 5.

transition region, i.e., they display the coupled nature of the magnetostructural phase transition. This coupling is also evident from the coinciding peaks of magnetic and strain susceptibility. Figure 12 indicates that for model II, we obtain the same temperature increase in ≈ 6 K with increasing external magnetic field H_{ext} from 0 to 5 T as for the simpler model I, agreeing with the experimentally observed shift of 1 K/T.[79]

The calculated temperature dependence of the magnetic part C_{mag} and total specific heat ($C=C_{mag}+C_{lat}$) of $Ni_{2.18}Mn_{0.82}Ga$ is shown in Figs. 13(a)–13(c). The lattice specific heat was calculated using the Debye model with $\Theta_D=328$ K (approximate value for N_2MnGa).[82] The results of simulation may be compared with available experimental data for some compositions ($x=0.18$, 0.19, and 0.24): the experimental total specific heat of $Ni_{2.19}Mn_{0.81}Ga$ in the absence of an external magnetic field[81] is presented in Fig. 13(d).

An interesting detail is revealed in Fig. 13(b), which shows the corresponding magnetic part of the specific heat in the absence of magnetoelastic coupling, i.e., for $J=U=K=0$, showing that it is considerably smaller than in presence of the coupling. The changes in the specific heat at T_{ms} have already been listed before (153, 145, and 132 J/(mol K) for $x=0.18$, 0.19, and 0.24, respectively). Our theoretical value of the zero-field specific heat change at T_{ms} in $Ni_{2.18}Mn_{0.82}Ga$ is ~ 160 J/(mol K) and comes fairly close to the experimental data.

Figure 14 shows the MC results for the magnetic entropy as a function of temperature for $Ni_{2.18}Mn_{0.82}Ga$ in various magnetic fields ($H_{ext}=0$ and 5 T) using Eq. (13) and $T_1=270$ and $T_2=383$ K. The saturation value of the entropy of $S_{mag}\approx 8$ J/(mol K) is almost consistent with the expected one [≈ 10.5 J/(mol K)] given by

$$S_{mag}=R\left\{\frac{N_{\mathrm{Mn}}}{N}\ln(2S_{\mathrm{Mn}}+1)+\frac{N_{\mathrm{Ni}}}{N}\ln(2S_{\mathrm{Ni}}+1)\right\}, \quad (24)$$

here, N is the total number of Ni and Mn atoms, N_{Mn} and N_{Ni} are the numbers of Mn and Ni atoms, respectively. As is obvious from Fig. 14, the theoretical curve of the entropy for $H_{ext}=0$ T exhibits a break at $T\approx 340$ K indicating the first-order character of the coupled magnetostructural phase transition.

Figure 15 displays the resulting isothermal magnetic entropy change ΔS_{mag} in $Ni_{2.18}Mn_{0.82}Ga$ as a function of temperature for varying magnetic fields from 0 to 5 T showing the importance of the magnetoelastic coupling term and comparing the result to the experimental data. As before, we assume that the structural contribution to the entropy does not change when changing the magnetic field. The experimental results for ΔS_{mag} have been obtained from isothermal magnetization measurements with the help of the Maxwell relation.[37] The discrepancy between the peak value of ΔS_{mag} obtained from Monte Carlo simulations and the peak value determined from the isothermal magnetization curves with the help of the Maxwell relation can be due to limited applicability of the latter to materials undergoing first-order magnetic phase transitions.[83] Nevertheless, the theoretical curve of entropy change follows qualitatively the experimental data although the absolute values cannot really be compared because we have integrated the specific-heat curves to obtain the entropy, i.e., Eq. (13) and (17), whereas the experimental entropy change has been obtained from Eq. (19).

Finally, the adiabatic temperature change is of interest with respect to any device exploiting the MCE. Table V lists ΔS_{mag}, ΔT_{mag}, and ΔT for $Ni_{2.18}Mn_{0.82}Ga$ and compares corresponding results obtained for model I and II. The temperature variation in theoretical and experimental adiabatic temperature changes is displayed in Figs. 16(a)–16(c). We notice that the comparison between theory and experiment is fairly well as long as ΔT is evaluated by using the full specific heat in Eq. (18).

V. DISCUSSION AND CONCLUSIONS

In this work, magnetostructural phase transitions and magnetocaloric properties of $Ni_{2+x}Mn_{1-x}Ga$ alloys have been studied by means of first principles and classical Monte Carlo simulations. First, the magnetic properties and magnetic energy scales have been determined by *ab initio* calculations of the magnetic exchange interaction parameters (Fig. 4), which also allowed to calculate the Curie temperature from first principles. Since the MCE of Ni-Mn-Ga alloys is most effective in the compositions range around $x=0.25$ where Curie and martensitic transformation temperatures merge together, we have included in the MC simulations, beside the magnetic degrees of freedom, also the tetragonal

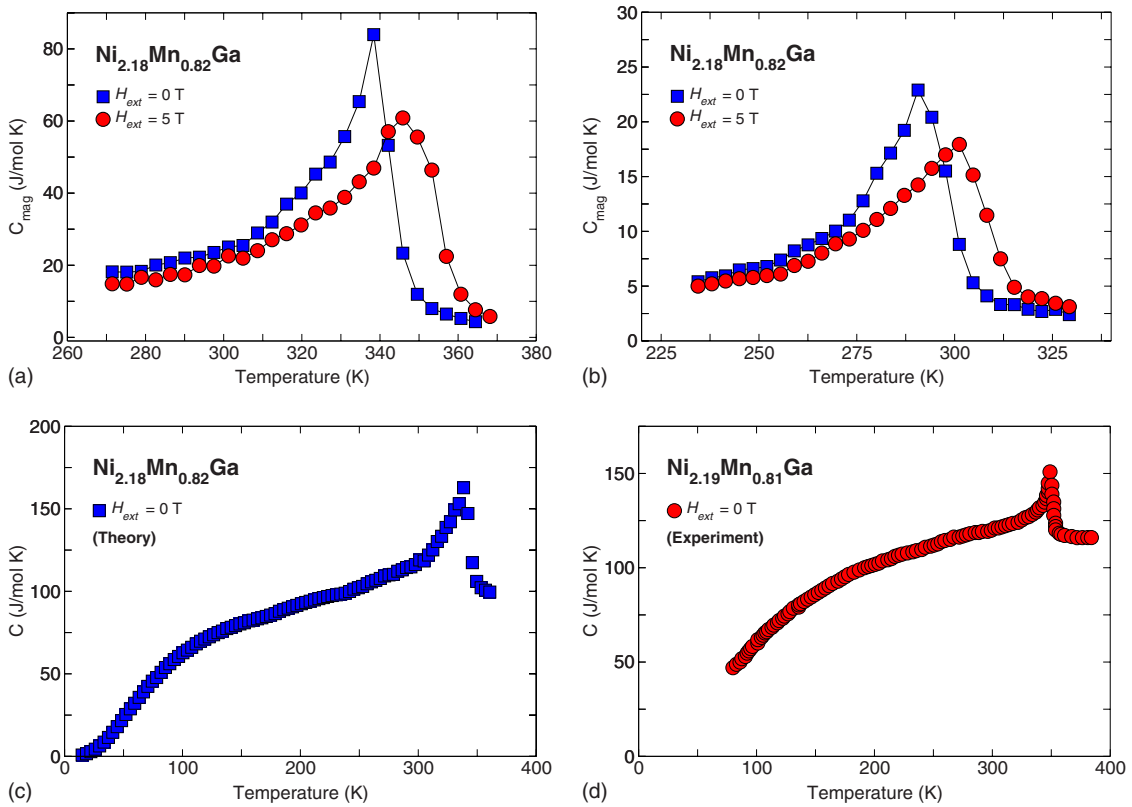

FIG. 13. (Color online) Monte Carlo results using model II for $Ni_{2.18}Mn_{0.82}Ga$: (a) the magnetic part of the specific heat, the lines with filled squares (blue), and filled circles (red) mark the magnetic specific heat in external magnetic field of 0 T and 5 T, respectively. (b) The magnetic part of the specific heat for the case that the magnetoelastic coupling is neglected showing that C_{mag} is smaller than in (a). (c) The total specific heat (sum of magnetic and lattice contributions with Θ_D=328 K) in the zero magnetic field. (d) The experimental result for the total specific heat of $Ni_{2.19}Mn_{0.81}Ga$ in zero magnetic field taken from Ref. 81.

distortions. The corresponding parameters in Eq. (11) involved in the changes in the crystal structure have not been determined by *ab initio* calculations but have been used as fit parameters to guarantee that T_C and T_m coincide in the corresponding compositional region centered at x=0.25.

Since the change in entropy in an external magnetic field around the first-order magnetostructural phase transition, $\Delta S_{mag}(T,H_{ext})$, plays a key role characterizing the *size* of the MCE, we have used instead of the simpler Heisenberg model an extended version of the Potts model allowing to simulate the magnetostructural phase transition and the temperature dependence of specific heat and entropy in a more adequate fashion. The entropy change has been obtained by integrating the specific-heat curves avoiding the use of the *magnetic* Clausius-Clapeyron equation.

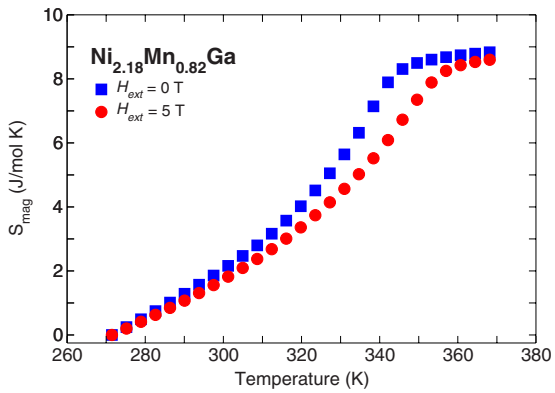

FIG. 14. (Color online) Monte Carlo simulation using model II of the temperature variation in the magnetic entropy of $Ni_{2.18}Mn_{0.82}Ga$. Filled squares (blue) and filled circles (red) mark the entropy variation in magnetic fields of H_{ext}=0 T and 5 T, respectively.

These investigations have been done for both kind of models, the simple cubic lattice (model I) and the realistic Heusler lattice (model II). For both models, the calculated MCE properties like the isothermal magnetic entropy change as well as the adiabatic temperature change upon variation in the magnetic field from 0 to 5 T, reproduce fairly well the experimental trends. However, fine tuning of simulation results (using the correct J_{ij}) is easier to achieve when using the real crystal structure of the Heusler systems.

To be more precise, in the fitting procedure, we have required that in the compositional range $0.18 \leq x \leq 0.27$ the Curie temperature T_C and the martensitic transition temperature T_m coincide, where T_C and T_m can be identified with the peak positions of the corresponding susceptibility curves. This is achieved by fixing the parameters K, K_1, and U. In spite of this fitting, the model is a powerful tool allowing to calculate rather accurately the maximum values of isothermal entropy and adiabatic temperature changes across the magnetostructural transition. *Accurately* means here that the

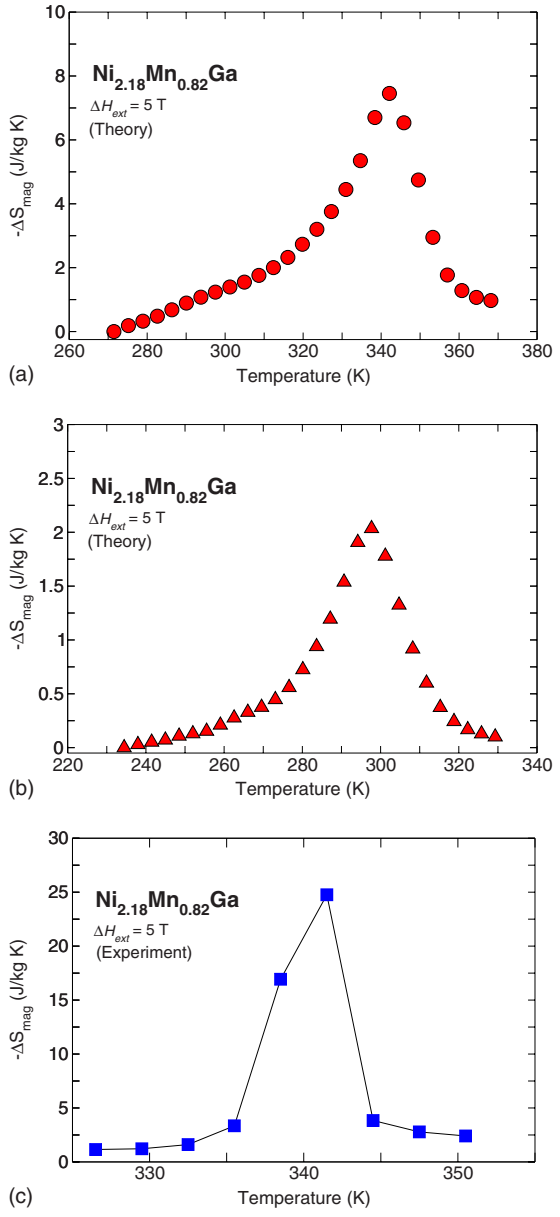

FIG. 15. (Color online) Monte Carlo results using model II showing (a) the isothermal magnetic entropy change ΔS_{mag} in $Ni_{2.18}Mn_{0.82}Ga$ upon variation in the magnetic field from 0 to 5 T in comparison to the (b) the corresponding entropy change in the absence of magnetoelastic coupling ($U=J=K=0$) and (c) experimental result of ΔS_{mag} in $Ni_{2.18}Mn_{0.82}Ga$ upon variation in the magnetic field from 0 to 5 T taken from Ref. 37.

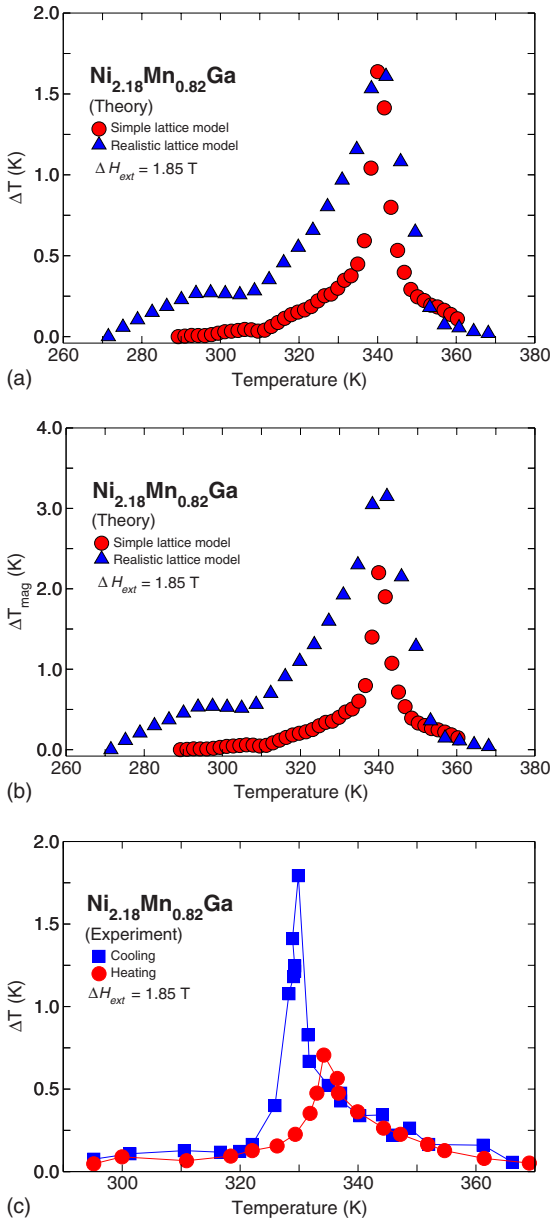

FIG. 16. (Color online) Monte Carlo results using model II for the adiabatic temperature change in $Ni_{2.18}Mn_{0.82}Ga$ upon variation in the magnetic field from 0 to 1.85 T for the case that (a) the full specific heat is used in Eq. (18) and (b) that only C_{mag} is retained in Eq. (18) in comparison with (c) the experimental result obtained from Ref. 37.

values of ΔS_{mag} and ΔT agree well in size with the experimental results. This agreement is greatly achieved by using the values of *ab initio* magnetic exchange parameters in the MC simulations (in an approximate way for the simple cubic lattice model and correctly for the Heusler lattice model).

Our investigations also show that the lattice contribution does not play an important role regarding the size of the isothermal entropy change, Eq. (17), across the magnetostructural transition as long as we may consider Θ_D not to depend too strongly on magnetization and the external magnetic field. At this point we cannot precise this further. Note that experiments on another Heusler alloy, Ni-Mn-In, have not shown an influence of the external magnetic field on the phonon dispersion so far, however, there seems to be some influence of the field on the elastic properties.[84] A weak influence of Θ_D with a correction term proportional to the square of the saturation magnetization has been discussed for ferromagnetic rare-earth metals.[85] However, in the present work, the lattice contribution to $\Delta S(T, H_{ext})$ is neglected.

Our simulations allow to study how a change in the magnetic interactions with composition will influence the MCE. The corresponding trend, when changing the composition, shows that with increasing x in $Ni_{2+x}Mn_{1-x}Ga$, T_{ms} increases as well as the size of $\Delta S_{mag}(T, H_{ext})$. Since this trend is also

TABLE V. Comparison of calculated MCE data for the simple cubic lattice (model I) and the Heusler lattice (model II) for the alloy $Ni_{2.18}Mn_{0.82}Ga$.

	ΔS_{mag} (J/mol K)	ΔT_{mag} (K)	ΔT (K)
	Model I		
$\Delta H_{ext}=1.85$ T	−1.86	2.20	1.63
$\Delta H_{ext}=5$ T	−3.33	3.93	2.93
	Model II		
$\Delta H_{ext}=1.85$ T	−0.78	3.15	1.6
$\Delta H_{ext}=5$ T	−1.8	7.37	3.7

accompanied with increasing antiferromagnetic tendencies, we may tentatively conclude that any enhancement of antiferromagnetic correlations due to atomic disorder or distortion in the ferromagnetic Heusler alloys will also enhance the MCE. Regarding this, Ni-Mn-Sb alloys may be good candidates exhibiting better MCE, i.e., higher ΔT. However, this prediction has to be taken with some care since any softening of the magnetic subsystem by admixture of antiferromagnetic correlations will also enhance the magnetic contribution to $C(T,H_{ext})$ in Eq. (18) so that the final effect on ΔT may be rather complex.

Nevertheless, calculations based on the Hamiltonian in Eq. (11) with *ab initio* input parameters may allow to predict whether a given material will display the conventional, inverse or both MCE.[86] The calculations can even predict the size of the MCE. So far, experimental trends in some of the systems listed in Table VI have been confirmed by our calculations. Further studies including an investigation of alloying *antiferromagnetically interacting species of atoms* are under way. In particular, there is one prerequisite for having a large MCE: A large shift in temperature of the martensitic transformation temperature either to larger or to lower temperatures under the influence of an external magnetic field is required. Table VI shows the change in T_m associated with the conventional MCE and inverse MCE observed for the Ni-Mn-(Ga, In, Sn, and Sb) alloys.

The magnetic field dependence of the martensitic transformation temperature and kinetic arrest in Ni-Mn-based Heusler alloys has been investigated in a series of papers. We cite here only a few results: for Ni-Mn-Ga the rate of change may be weak (≈1–3 K/T) (Refs. 70, 87, and 88) or strong

TABLE VI. Positive or negative change in the martensitic transformation temperature T_m under the action of an external magnetic field for the Ni-Mn-(Ga, In, Sn, and Sb) alloys in K/T (see text for references).

Heusler alloy	Change in T_m (K/T)
Ni-Mn-Ga	+(1–6)
Ni-Mn-In	−(10–11)
Ni-Mn-Sn	−(1–3)
Ni-Mn-Sb	−(1–3)

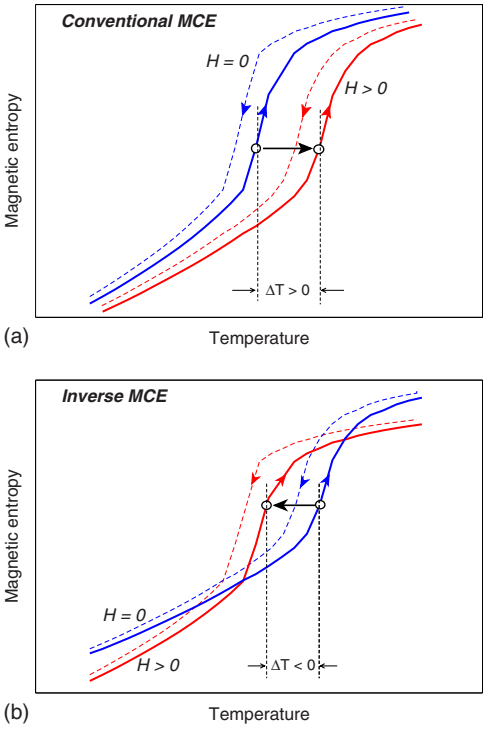

FIG. 17. (Color online) Qualitative sketch of the isothermal entropy as a function of temperature around a first-order phase transformation for zero and finite external magnetic field, showing the adiabatic temperature changes associated with the conventional and inverse magnetocaloric effect, respectively.

(≈6 K/T);[89] for Ni-Mn-In it is large (≈10–11 K/T);[90] for Ni-Mn-Sn and Ni-Mn-Sb it is weak, (≈1–3 K/T).[74,91] The Ni-Mn-Ga alloys in Table VI exhibit only two phases, paramagnetic austenite and ferromagnetic martensite, i.e., there is no ferromagnetic austenite. The alloy with the strong rate of change (6 K/T) investigated by Jeong *et al.*[89] is $Ni_{2.14}Mn_{0.78}Ga_{1.08}$.

In experiment, the shift of T_m is determined with some error because the jump of the magnetization at T_m may be rather broad. But for all alloys, the adiabatic temperature change around the first-order phase transformation clearly allows to distinguish the conventional MCE (positive ΔT) from the inverse MCE (negative ΔT).

A particularly interesting effect is connected with additional alloying, not investigated in the present work, which may change T_m drastically. For instance, the addition of Co in $Ni_{45}Co_5Mn_{36.7}In_{13.3}$ has been found sufficient to suppress T_m in a magnetic field of 8 T.[92] Such alloying effects in order to achieve a maximum shift of T_m in a magnetic field in order to optimize the MCE, will be studied later. Substantial alloying effects have also been found when substituting small amounts of Ga for In in $Ni_{50}Mn_{34}In_{16}$ thereby shifting the technically important properties close to room temperature.[93]

On the basis of calculations of *ab initio* magnetic exchange interaction parameters of Ni-Mn-Ga alloys, we can make some tentative prediction for new magnetic Heusler alloys, which may show better MCE effects. For example, we expect from substituting Ni by a few percent by ferromagnetic elements such as Co (or appropriate rare earth el-

ements) will increase the positive rate of change in T_m with the external magnetic field. This may be related to the enhancement of the ferromagnetic nature of correlations in the martensitic state. On the other hand, an increase in the inverse MCE may be achieved by, as the experiment in Ref. 92 suggests, adding Co and Mn to the Ni-Mn-(In. Sn, Sb) alloys, which will enhance the ferromagnetic correlations in austenite and increase the antiferromagnetic correlations in martensite.

In search for alloys with better MCE, it may be useful to have a look at the qualitative change in the entropy over the temperature range which includes the first-order martensitic transformation. This is sketched in Figs. 17(a) and 17(b) for the conventional and inverse MCE. The idea of substitutional alloying is to enhance the ferromagnetic correlations in the martensitic state and simultaneously weaken these correlations in the austenitic state which will enhance the conventional MCE. The reverse, enhancing the ferromagnetic correlations in the austenitic state, will lead to an increase in the inverse MCE. In this context, see also the discussion in two recent review articles.[32,94]

In summary, the 3-5-state Potts used here to describe the mutual influence of magnetic and martensitic transitions, allows predictive statements regarding the search for magnetic Heusler alloys exhibiting a larger MCE although this has to be checked by calculations in each case. For this fine tuning of theoretical modeling, the full Heusler lattice model is superior to the simpler cubic lattice model.

ACKNOWLEDGMENTS

This work was supported by RFBR under Grants No. 06-02-39030-NNSF, No. 07-02-96029-r-ural, No. 07-02-13629-OFI–ts, and No. 08-02-91317, by Ministry of Education and Science of the Russian Federation (Grants No. NK-421P-71), and by SPP 1239 (DFG, Germany). P. Entel would like to thank Lluis Mañosa for helpful discussions.

[1] K. A. Gschneidner, Jr. and V. K. Pecharsky, Int. J. Refrig. **31**, 945 (2008).
[2] V. K. Pecharsky and K. A. Gschneidner, Jr., Phys. Rev. Lett. **78**, 4494 (1997).
[3] O. Tegus, E. Brück, K. H. J. Buschow, and F. R. de Boer, Nature (London) **415**, 150 (2002).
[4] K. A. Gschneidner, Jr., V. K. Pecharsky, and A. O. Tsokol, Rep. Prog. Phys. **68**, 1479 (2005).
[5] J. S. Amaral, N. J. O. Silva, and V. S. Amaral, Appl. Phys. Lett. **91**, 172503 (2007).
[6] C. Triguero, M. Porta, and A. Planes, Phys. Rev. B **73**, 054401 (2006).
[7] C. Triguero, M. Porta, and A. Planes, Phys. Rev. B **76**, 094415 (2007).
[8] E. P. Nobrega, N. A. de Oliveira, P. J. von Ranke, and A. Troper, Phys. Rev. B **72**, 134426 (2005).
[9] E. P. Nobrega, N. A. de Oliveira, P. J. von Ranke, and A. Troper, J. Phys.: Condens. Matter **18**, 1275 (2006).
[10] E. P. Nobrega, N. A. de Oliveira, P. J. von Ranke, and A. Troper, J. Appl. Phys. **99**, 08Q103 (2006).
[11] E. P. Nobrega, N. A. de Oliveira, P. J. von Ranke, and A. Troper, Phys. Rev. B **74**, 144429 (2006).
[12] E. P. Nobrega, N. A. de Oliveira, P. J. von Ranke, and A. Troper, Physica B **378-380**, 716 (2006).
[13] E. P. Nobrega, N. A. de Oliveira, P. J. von Ranke, and A. Troper, J. Magn. Magn. Mater. **310**, 2805 (2007).
[14] L. G. de Medeiros, Jr. and N. A. de Oliveira, J. Magn. Magn. Mater. **306**, 265 (2006).
[15] P. J. von Ranke, S. Gama, A. A. Coelho, A. de Campos, A. M. G. Carvalho, F. C. G. Gandra, and N. A. de Oliveira, Phys. Rev. B **73**, 014415 (2006).
[16] E. Bruck, O. Tegus, D. T. Cam Thanh, N. T. Trung, and K. H. J. Buschow, Int. J. Refrig. **31**, 763 (2008).
[17] L. Pareti, M. Solzi, F. Albertini, and A. Paoluzi, Eur. Phys. J. B **32**, 303 (2003).
[18] F. Albertini, F. Canepa, S. Cirafici, E. A. Franceschi, M. Napoletano, A. Paoluzi, L. Pareti, and M. Solzi, J. Magn. Magn. Mater. **272-276**, 2111 (2004).
[19] A. Aliev, A. Batdalov, S. Bosko, V. Buchelnikov, I. Dikshtein, V. Khovailo, V. Koledov, R. Levitin, V. Shavrov, and T. Takagi, J. Magn. Magn. Mater. **272-276**, 2040 (2004).
[20] X. Zhou, W. Li, H. P. Kunkel, and G. Williams, J. Phys.: Condens. Matter **16**, L39 (2004).
[21] M. Pasquale, C. P. Sasso, L. H. Lewis, L. Giudici, T. Lograsso, and D. Schlagel, Phys. Rev. B **72**, 094435 (2005).
[22] F. Albertini, A. Paoluzi, L. Pareti, M. Solzi, L. Righi, E. Villa, S. Besseghini, and F. Passaretti, J. Appl. Phys. **100**, 023908 (2006).
[23] V. D. Buchelnikov, S. V. Taskaev, A. M. Aliev, A. B. Batdalov, A. M. Gamzatov, A. V. Korolyov, N. I. Kourov, V. G. Pushin, V. V. Koledov, V. V. Khovailo, V. G. Shavrov, and R. M. Grechishkin, Int. J. Appl. Electromagn. Mech. **23**, 65 (2006).
[24] S. Stadler, M. Khan, J. Mitchell, N. Ali, A. M. Gomes, I. Dubenko, A. Y. Takeuchi, and A. P. Guimaraes, Appl. Phys. Lett. **88**, 192511 (2006).
[25] F. Albertini, J. Kamarad, Z. Arnold, L. Pareti, E. Villa, and L. Righi, J. Magn. Magn. Mater. **316**, 364 (2007).
[26] J. F. Duan, P. Huang, H. Zhang, Y. Long, G. H. Wu, R. C. Ye, Y. Q. Chang, and F. R. Wan, J. Alloys Compd. **441**, 29 (2007).
[27] M. Khan, I. Dubenko, S. Stadler, and N. Ali, J. Appl. Phys. **102**, 023901 (2007).
[28] F. Albertini, M. Solzi, A. Paoluzi, and L. Righi, Mater. Sci. Forum **583**, 169 (2008).
[29] J. F. Duan, Y. Long, B. Bao, H. Zhang, R. C. Ye, Y. Q. Chang, F. R. Wan, and G. H. Wu, J. Appl. Phys. **103**, 063911 (2008).
[30] V. V. Khovaylo, K. P. Skokov, Yu. S. Koshkid'ko, V. V. Koledov, V. G. Shavrov, V. D. Buchelnikov, S. V. Taskaev, H. Miki, T. Takagi, and A. N. Vasiliev, Phys. Rev. B **78**, 060403(R) (2008).
[31] C. P. Sasso, M. Kuepferling, L. Giudici, V. Basso, and M. Pasquale, J. Appl. Phys. **103**, 07B306 (2008).
[32] A. Planes, L. Mañosa, and M. Acet, J. Phys.: Condens. Matter **21**, 233201 (2009).

[33] P. J. Webster, K. R. A. Ziebeck, S. L. Town, and M. S. Peak, Philos. Mag. B **49**, 295 (1984).
[34] A. N. Vasil'ev, A. D. Bozhko, V. V. Khovailo, I. E. Dikshtein, V. G. Shavrov, V. D. Buchel'nikov, M. Matsumoto, S. Suzuki, T. Takagi, and J. Tani, Phys. Rev. B **59**, 1113 (1999).
[35] V. V. Khovaylo, V. D. Buchelnikov, R. Kainuma, V. V. Koledov, M. Ohtsuka, V. G. Shavrov, T. Takagi, S. V. Taskaev, and A. N. Vasiliev, Phys. Rev. B **72**, 224408 (2005).
[36] S. Banik, A. Chakrabarti, U. Kumar, P. K. Mukhopadhyay, A. M. Awasthi, R. Ranjan, J. Schneider, B. L. Ahuja, and S. R. Barman, Phys. Rev. B **74**, 085110 (2006).
[37] V. Khovaylo, V. Koledov, V. Shavrov, A. Korolyov, K. Skokov, M. Ohtsuka, H. Miki, and T. Takagi, in *Refrigeration Science and Technology Proceedings, 2nd International Conference on Magnetic Refrigeration at Room Temperature*, Portoroz, Slovenia (International Institute of Refrigeration, Comissions B2, A1 with E2, Paris, France, 2007), p. 217.
[38] P. Entel, V. D. Buchelnikov, V. V. Khovailo, A. T. Zayak, W. A. Adeagbo, M. E. Gruner, H. C. Herper, and E. F. Wassermann, J. Phys. D **39**, 865 (2006).
[39] J. P. Perdew, K. Burke, and M. Ernzerhof, Phys. Rev. Lett. **77**, 3865 (1996).
[40] P. E. Blöchl, Phys. Rev. B **50**, 17953 (1994).
[41] G. Kresse and D. Joubert, Phys. Rev. B **59**, 1758 (1999).
[42] G. Kresse and J. Furthmüller, Phys. Rev. B **54**, 11169 (1996).
[43] S. Banik, R. Ranjan, A. Chakrabarti, S. Bhardwaj, N. P. Lalla, A. M. Awasthi, V. Sathe, D. M. Phase, P. K. Mukhopadhyay, D. Pandey, and S. R. Barman, Phys. Rev. B **75**, 104107 (2007).
[44] A. I. Liechtenstein, M. I. Katsnelson, and V. A. Gubanov, J. Phys. F: Met. Phys. **14**, L125 (1984).
[45] A. I. Liechtenstein, M. I. Katsnelson, V. P. Antropov, and V. A. Gubanov, J. Magn. Magn. Mater. **67**, 65 (1987).
[46] H. Ebert, in *Electronic Structure and Physical Properties of Solids*, Lecture Notes in Physics Vol. 535, edited by H. Dreyssé (Springer, Berlin, 1999), p. 191; Rep. Prog. Phys. **59**, 1665 (1996).
[47] H. Akai and P. H. Dederichs, Phys. Rev. B **47**, 8739 (1993).
[48] D. Ködderitzsch, H. Ebert, D. A. Rowlands, and A. Ernst, New J. Phys. **9**, 81 (2007).
[49] V. D. Buchelnikov, P. Entel, S. V. Taskaev, V. V. Sokolovskiy, A. Hucht, M. Ogura, H. Akai, M. E. Gruner, and S. K. Nayak, Phys. Rev. B **78**, 184427 (2008).
[50] S. Aksoy, M. Acet, P. P. Deen, L. Mañosa, and A. Planes, Phys. Rev. B **79**, 212401 (2009).
[51] J. Thoene, S. Chadov, G. Fecher, C. Felser, and J. Kübler, J. Phys. D **42**, 084013 (2009).
[52] V. V. Khovaylo, T. Kanomata, T. Tanaka, M. Nakashima, Y. Amako, R. Kainuma, R. Y. Umetsu, H. Morito, and H. Miki, Phys. Rev. B **80**, 144409 (2009).
[53] R. Y. Umetsu, R. Kainuma, Y. Amako, Y. Taniguchi, T. Kanomata, K. Fukushima, A. Fujita, K. Oikawa, and K. Ishida, Appl. Phys. Lett. **93**, 042509 (2008).
[54] S. V. Okatov, A. R. Kuznetsov, Yu. N. Gornostyrev, V. N. Urtsev, and M. I. Katsnelson, Phys. Rev. B **79**, 094111 (2009).
[55] M. E. Gruner, P. Entel, I. Opahle, and M. Richter, J. Mater. Sci. **43**, 3825 (2008).
[56] J. Enkovaara, A. Ayuela, L. Nordström, and R. M. Nieminen, Phys. Rev. B **65**, 134422 (2002).
[57] A. Sozinov, A. A. Likhachev, and K. Ullakko, IEEE Trans. Magn. **38**, 2814 (2002).
[58] O. Heczko, L. Straka, N. Lanska, and K. Ullakko, J. Appl. Phys. **91**, 8228 (2002).
[59] O. N. Mryasov, U. Nowak, K. Y. Guslienko, and R. W. Chantrell, Europhys. Lett. **69**, 805 (2005).
[60] M. Ležaić, Ph. Mavropoulos, J. Enkovaara, G. Bihlmayer, and S. Blügel, Phys. Rev. Lett. **97**, 026404 (2006).
[61] M. E. Gruner, E. Hoffmann, and P. Entel, Phys. Rev. B **67**, 064415 (2003).
[62] B. L. Ahuja, B. K. Sharma, S. Mathur, N. L. Heda, M. Itou, A. Andrejczuk, Y. Sakurai, A. Chakrabarti, S. Banik, A. M. Awasthi, and S. R. Barman, Phys. Rev. B **75**, 134403 (2007).
[63] F. Y. Wu, Rev. Mod. Phys. **54**, 235 (1982).
[64] C. Choi, J. Kim, and S. Kim, J. Korean Phys. Soc. **46**, 562 (2005).
[65] M. Blume, V. J. Emery, and R. B. Griffiths, Phys. Rev. A **4**, 1071 (1971).
[66] E. Vives, T. Castán, and P.-A. Lindgård, Phys. Rev. B **53**, 8915 (1996).
[67] T. Cástan, E. Vives, and P.-A. Lindgård, Phys. Rev. B **60**, 7071 (1999).
[68] T. W. Burkhardt, Phys. Rev. B **60**, 12502 (1999).
[69] D. K. Ray and J. P. Jardin, Phys. Rev. B **33**, 5021 (1986).
[70] V. V. Khovailo, V. Novosad, T. Takagi, D. A. Filippov, R. Z. Levitin, and A. N. Vasilev, Phys. Rev. B **70**, 174413 (2004).
[71] T. Krenke, M. Acet, E. F. Wassermann, X. Moya, L. Mañosa, and A. Planes, Phys. Rev. B **73**, 174413 (2006).
[72] A. M. Tishin and Y. I. Spichkin, *The Magnetocaloric Effect and Its Applications*, IOP Series in Condensed Matter Physics, edited by J. M. D. Coey, D. R. Tilley, and D. R. Vij (IOP, Bristol, 2003).
[73] T. Krenke, E. Duman, M. Acet, E. F. Wassermann, X. Moya, L. Mañosa, and A. Planes, Nature Mater. **4**, 450 (2005).
[74] X. Moya, L. Mañosa, A. Planes, S. Aksoy, M. Acet, E. F. Wassermann, and T. Krenke, Phys. Rev. B **75**, 184412 (2007).
[75] A. Zheludev, S. M. Shapiro, P. Wochner, A. Schwartz, M. Wall, and L. E. Tanner, Phys. Rev. B **51**, 11310 (1995).
[76] U. Stuhr, P. Vorderwisch, V. V. Kokorin, and P.-A. Lindgard, Phys. Rev. B **56**, 14360 (1997).
[77] V. D. Buchelnikov, V. V. Khovailo, and T. Takagi, J. Magn. Magn. Mater. **300**, e459 (2006).
[78] D. P. Landau and K. Binder, *A Guide to Monte Carlo Simulations in Statistical Physics* (Cambridge Univesity Press, Cambridge, 2000).
[79] I. E. Dikshtein, D. I. Ermakov, V. V. Koledov, L. V. Koledov, T. Takagi, A. A. Tulaikova, A. A. Cherechukin, and V. G. Shavrov, JETP Lett. **72**, 373 (2000).
[80] Y. K. Kuo, K. M. Sivakumar, H. C. Chen, J. H. Su, and C. S. Lue, Phys. Rev. B **72**, 054116 (2005).
[81] T. Kanomata, *Proceedings of International Seminar on Shape Memory Alloys and Related Technologies*, Sendai, Japan (Institute of Fluid Science, Tohoku University, Sendai, Japan, 1999), p. 12.
[82] See Table I in M. Kreissl, K.-U. Neumann, T. Stephens, and K. R. A. Ziebeck, J. Phys.: Condens. Matter **15**, 3831 (2003).
[83] J. S. Amaral and V. S. Amaral, Appl. Phys. Lett. **94**, 042506 (2009).
[84] L. Mañosa, A. Planes, X. Moya, D. Gonzalez-Alonso, O. Garlea, T. Lograsso, D. Schlage, J. Zarestky, S. Aksoy, and M. Acet, European Symposium on Martensitic Transformations, 2009, Prague, Czech Republic (unpublished), No. A1.02.

[85] V. Yu. Bodryakov, A. A. Povzneer, and O. G. Zeyukova, Phys. Solid State **41**, 1138 (1999).
[86] V. D. Buchelnikov, V. V. Sokolovskiy, S. V. Taskaev, and P. Entel, Mater. Sci. Forum **635**, 137 (2010).
[87] D. A. Filippov, V. V. Khovailo, V. V. Koledov, E. P. Krasnoperov, R. Z. Levitin, V. G. Shavrov, and T. Takagi, J. Magn. Magn. Mater. **258-259**, 507 (2003).
[88] J. H. Kim, F. Inaba, T. Fukuda, and T. Kakeshita, Acta Mater. **54**, 493 (2006).
[89] S. Jeong, K. Inoue, S. Inoue, K. Koterazawa, M. Taya, and K. Inoue, Mater. Sci. Eng., A **359**, 253 (2003).
[90] T. Krenke, E. Duman, M. Acet, E. F. Wassermann, X. Moya, L. Mañosa, A. Planes, E. Suard, and B. Ouladdiaf, Phys. Rev. B **75**, 104414 (2007).
[91] K. Koyama, H. Okada, K. Watanabe, T. Kanomata, R. Kainuma, W. Ito, K. Oikawa, and K. Ishida, Appl. Phys. Lett. **89**, 182510 (2006).
[92] W. Ito, K. Ito, R. Y. Umetsu, R. Kainuma, K. Koyama, K. Watanabe, A. Fujita, K. Oikawa, K. Ishida, and T. Kanomata, Appl. Phys. Lett. **92**, 021908 (2008).
[93] S. Aksoy, T. Krenke, M. Acet, E. F. Wassermann, X. Moya, L. Mañosa, and A. Planes, Appl. Phys. Lett. **91**, 241916 (2007).
[94] M. Acet, L. Mañosa, and A. Planes (unpublished).